FDL-TDR-64-120

[redacted]

$2.00

PRESSURE AND HEAT TRANSFER MEASUREMENTS FOR MACH 21 FLOWS OVER A BLUNT PYRAMIDAL CONFIGURATION WITH AERODYNAMIC CONTROLS

PART OF AN INVESTIGATION OF HYPERSONIC FLOW SEPARATION AND CONTROL CHARACTERISTICS

AD 609553

TECHNICAL DOCUMENTARY REPORT No. FDL-TDR-64-120

49 p
COPY 2 OF 3
HARD COPY $.2.00
MICROFICHE $.0.50

AUGUST 1964

AF FLIGHT DYNAMICS LABORATORY
RESEARCH AND TECHNOLOGY DIVISION
AIR FORCE SYSTEMS COMMAND
WRIGHT-PATTERSON AIR FORCE BASE, OHIO

DDC
RELEASED
OCT 19 1964
DDC-IRA A

Project No. 8219, Task No. 821902

(Prepared under Contract No. AF 33(616)-8130 by
Grumman Aircraft Engineering Corporation, Bethpage, New York;
Author: Louis G. Kaufman II)

ARCHIVE COPY

NOTICES

When Government drawings, specifications, or other data are used for any purpose other than in connection with a definitely related Government procurement operation, the United States Government thereby incurs no responsibility nor any obligation whatsoever; and the fact that the Government may have formulated furnished, or in any way supplied the said drawings, specifications, or other data, is not to be regarded by implication or otherwise as in any manner licensing the holder or any other person or corporation, or conveying any rights or permission to manufacture, use, or sell any patented invention that may in any way be related thereto.

Qualified requesters may obtain copies of this report from the Defense Documentation Center (DDC), (formerly ASTIA), Cameron Station, Bldg. 5, 5010 Duke Street, Alexandria, Virginia, 22314.

This report has been released to the Office of Technical Services, U.S. Department of Commerce, Washington 25, D. C., in stock quantities for sale to the general public.

Copies of this report should not be returned to the Research and Technology Division, Wright-Patterson Air Force Base, Ohio, unless return is required by security considerations, contractual obligations, or notice on a specific document.

500 - September 1964 - 448-5-151

FOREWORD

This report presents results of a portion of the experimental program for the investigation of hypersonic flow separation and control characteristics being conducted by the Research Department of Grumman Aircraft Engineering Corporation, Bethpage, New York. Messrs. Donald E. Hoak and Wilfred J. Klotzback, of the Flight Control Division, Air Force Flight Dynamics Laboratory, Research and Technology Division, located at Wright-Patterson Air Force Base, Ohio, are the Air Force Project Engineers for the program, which is being supported partly under Contract AF 33(616) 8130, Air Force Project No. 8219, Task No. 821902.

ABSTRACT

Pressure and heat transfer data were obtained for Mach 21 flows over a blunt pyramidal configuration composed of a 70 degree sweepback delta wing surface and two dihedral surfaces. Instrumented trailing edge flaps were mounted in pairs on either the delta wing or dihedral surfaces and an uninstrumented ventral fin was attached during several test runs. The model was pitched at angles of attack between -30 and +45 degrees for free stream Reynolds numbers, based on model length, of approximately 51,000.

This report has been reviewed and is approved.

W. A. SLOAN, JR.
COL. USAF
Actg Chief, Flight Control Division
Air Force Flight Dynamics Laboratory

TABLE OF CONTENTS

LIST OF ILLUSTRATIONS

LIST OF SYMBOLS

C_p	pressure coefficient, $C_p \equiv (p - p_\infty)/q_\infty$
h	heat transfer coefficient (BTU/ft^2 sec ^oR), $h \equiv \dot{q}_w/(T_o - T_w)$
k	thermal conductivity of free stream flow (BTU/ft sec ^oR)*
M	Mach number
M_∞	free stream Mach number*
Nu	Nusselt number, $Nu \equiv hx/k$
p	pressure (psia)
p_o	stagnation pressure (psia)
p_∞	free stream static pressure (psia)*
$\dot{q}_w$	aerodynamic heating rate (BTU/ft^2 sec)
q_∞	free stream dynamic pressure (psia)*
Re_x	Reynolds number based on x, $Re_x \equiv \rho_\infty U_\infty x/\mu_\infty$
Re_∞/ft	Reynolds number per foot, $Re_\infty/ft \equiv \rho_\infty U_\infty/\mu_\infty$
t	time (sec)
T	temperature (^oR)
T_o	stagnation temperature (^oR)
T_w	wall temperature (^oR)

T_∞ free stream static temperature (^oR)*

U_∞ free stream velocity (ft/sec)*

x streamwise distance from virtual apex to planform projection of thermocouple, $x \equiv \frac{8.325 \text{ in.}}{12 \text{ in./ft}} X'$ (see Fig. 4)

X' nondimensional streamwise distance from virtual apex to planform projection (see Fig. 4)

Y' nondimensional spanwise distance measured outboard from the model centerline

α angle of attack (degrees)

μ_∞ viscosity of air in the free stream (slugs/ft sec)*

ρ_∞ density of air in the free stream (slugs/ft^3)*

*Reference values for these "free stream" properties are calculated for each run at the sector center of rotation, 7.00 inches downstream of conical nozzle exit on the tunnel axis.

INTRODUCTION

The experimental data generated for an investigation of hypersonic flow separation and aerodynamic control characteristics are presented in a series of reports, of which this is one. Pressure, heat transfer and force data were obtained for hypersonic flows over "basic geometries," such as a wedge mounted on a flat plate, and for "typical" hypersonic flight configurations with aerodynamic control surfaces. The experimental portion of the program required a total of 11 models (see Fig. 1, p. 13); 8 for tests in the von Karman Facility of the Arnold Engineering Development Center and 3 for tests in the Grumman Hypersonic Shock Tunnel (GHST) (Refs. 1 and 2). Analyses of the entire test program are to be presented in a forthcoming final report on the investigation of hypersonic flow separation and control characteristics.

This report presents pressure and heat transfer data obtained during April 1964 in the GHST (Ref. 3) on a blunt pyramidal configuration having attachable trailing edge flaps. Geometrically similar models, one instrumented for force measurements and the other instrumented for pressure and heat transfer measurements, were tested in the AEDC 40-inch supersonic and 50-inch Mach 8 tunnels (see Fig. 1).

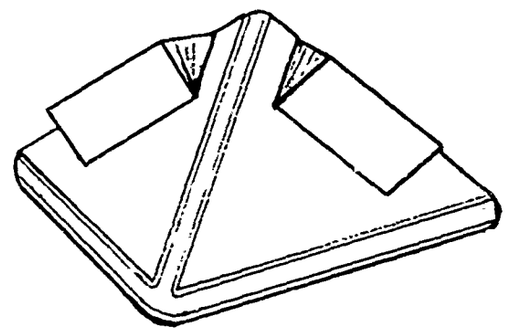

MODEL

Photographs of the model installed in the GHST are shown in Figs. 2 and 3. The lower surface of the model is a blunt delta wing with 70 degree sweepback. The planar portions of the dihedral upper surfaces are right triangles and are connected by a cylindrical segment which forms the model's "ridge line." The three cylindrical leading edges and the spherical nose have the same radius.

Manuscript released by the author in May 1964 for publication as an FDL Technical Documentary Report.

The cross-sectional shape is the same as one of the ASD — General Applied Sciences Laboratory pyramidal models tested in the AEDC Hotshot 2 hypervelocity facility (Ref. 4).

The model has four attachable trailing edge flaps, one on each dihedral surface (shown attached in Fig. 3), and two on the lower surface of the model. The flaps are always mounted in pairs, either both dihedral (upper) surface flaps or both lower surface flaps are attached to the model. As shown in Figs. 4 and 5, the flaps have rectangular planforms, and their hinge lines are parallel to the base of the model (perpendicular to the ridge line). The flap chords are 15 per cent of the virtual length of the model and the "deflection" angles of the attachable flaps are 40 degrees, measured in the planes normal to the flap hinge lines.

An uninstrumented ventral fin is attachable to the lower surface of the model between the trailing edge flaps (Figs. 4 and 5). The wedge shaped fin has a total wedge angle of 30 degrees, a cylindrical leading edge, and a chord equal to 15 per cent of the model reference length. The ventral fin is geometrically similar to the instrumented fin of Configuration "B" shown in Fig. 1.

The attachable flaps and fin provide four model configurations: 1) the basic configuration, 2) the basic configuration + the lower surface flaps, 3) the basic configuration + the upper surface flaps, and 4) the basic configuration + the ventral fin.

Twelve pressure transducers and eight heat transfer gauges are mounted in the model at the locations shown in Fig. 4 (see also Table I). The gauges are positioned along streamwise lines coincident with the flap centerlines and extending forward to the leading edges of the model. Two pressure gauge taps are on the model leading edges. Another two are on the lower surface centerline; the downstream one is covered when the ventral fin is attached. The pressure and heat transfer gauges in the attachable flaps and the corresponding gauges in the basic model, (which are covered when the flaps are attached), are equidistant from the flap "hinge lines."

TEST CONDITIONS

The model was tested at angles of attack of: -30, -15, 0, +14.3, +30 and +45 degrees. Angles of attack, α , are referenced to the lower, delta wing, surface of the model and are positive when this surface is windward. At $\alpha = +14.3^{o}$ the dihedral surfaces are parallel to the free stream flow and all flap hinge lines are perpendicular to the free stream flow direction. The model configurations tested at the various angles of attack are indicated in Table II.

Useful test flow durations of approximately 3 milliseconds were obtained in the Grumman Hypersonic Shock Tunnel (GHST) for the tunnel flow conditions given in Table III. The 25 degree, total angle, conical nozzle used had an exit diameter of 18 inches and an exit Mach number of 19. It provided Mach 21 flow with free stream Reynolds numbers, Re_{∞}, of approximately 73,000 per foot in the region of the model instrumentation. Because the flow was conical, stream conditions varied in the test section with distance, both along and away from the tunnel centerline. Distributions of the Mach number and static to total pressure and temperature ratios are plotted in Fig. 6 versus axial distance downstream of the nozzle exit. These distributions, obtained from the calibration of the tunnel nozzle, were taken as invariant from run to run.

Although the calibration curves are invariant, the tunnel stagnation and free stream static conditions vary from run to run. Reference free stream static conditions, at a station 7.00 inches downstream of the nozzle exit, are given in Table III for each test run. Corresponding values of the stagnation pressure and temperature and axial distributions of the static conditions can be calculated for each run by using the calibration curves presented in Fig. 6.

Schlieren flow photographs were taken during several test runs, for angles of attack from 0 to +45 degrees. Even at the highest angle of attack, however, the low density of the stream flow greatly limited the usefulness of the schlieren flow photographs.

DATA REDUCTION AND ACCURACY

Pressure and heat transfer data were reduced to the standard coefficient forms presented herein by using reference "free stream" conditions. These were taken as those at the tunnel sector center of rotation, (7.00 inches downstream of nozzle exit). As shown in Figs. 4 and 6, the center of rotation is in the aft portion of the model in the vicinity of the pressure and heat transfer gauges.*

Measured pressures, p, were reduced to pressure coefficients,

$$C_p = \frac{p - p_\infty}{q_\infty} ,$$

using the reference free stream values of the static and dynamic pressures, p_∞ and q_∞, calculated at the sector center of rotation for each test run.

Aerodynamic heating rates, $\dot{q}_w$, were presented directly by the heat transfer gauge instruments (from measurements of the transient wall temperatures, T_w). The heating rates were nondimensionalized in the form

$$\frac{Nu}{\sqrt{Re_x}} = \left(\frac{\dot{q}_w}{T_o - T_w}\right)\left(\frac{x}{k}\right)\sqrt{\frac{\rho_\infty U_\infty x}{\mu_\infty}}$$

where Nu is the Nusselt number, x is the streamwise distance from the virtual apex to the planform projection of the heat transfer gauge (see Table I and Fig. 4), and Re_x is the Reynolds number based on distance x. For each test run, the values of k, ρ_∞, U_∞, and μ_∞ (the thermal conductivity, density, velocity and viscosity of the free stream flow), were calculated at the sector center of rotation. Values of k and Re_∞, ($Re_x = xRe_\infty$), are given in Table III for each test run.

*At $\alpha = 0$, the center of rotation is at $X' = 0.6246$ (X' is the nondimensional model coordinate measured downstream from the planform virtual apex).

The proximity of the pressure and heat transfer gauges to the chosen reference point for the free stream conditions minimizes corrections due to the nonuniformity of the tunnel flow. Because of the blunt shape of the model and the high pressure levels, neither "buoyancy" (Ref. 3) nor "flow angularity" corrections are justified for the data presented herein.*

Pressures and heating rates were estimated to be accurate to within 10 percent of their measured values. In addition to these estimates, the model configurations and test conditions provide a certain amount of repeatability which can be used to ascertain the accuracy of the data presented herein for the basic configuration. Thus, for example, the upper surface data should not be influenced by the addition of the ventral fin to the lower surface.

RESULTS

Table II summarizes the data obtained on the model and indicates the corresponding figure numbers where the data are presented herein. The GHST test run numbers given in the table indicate the order in which the data were obtained and are to be used when referring to the tabulated values of the free stream reference conditions given in Table III. The omission of test run numbers indicates gauge calibration or faulty test runs.

The pressure and heat transfer data, in coefficient form, are plotted in Figs. 7 through 27. Pressure coefficients and values of $Nu/\sqrt{Re_x}$ are plotted versus X', nondimensional streamwise distance downstream of the planform virtual apex of the model (see Table I and Fig. 4). The reference free stream conditions for the coefficients are those at the tunnel sector center of rotation (at X' = 0.6246 for $\alpha = 0$). Data obtained from the gauges mounted in the flaps are plotted at the X' stations of the corresponding gauges in the basic model.

---

*For example, the "buoyancy" correction for the axial variation in the tunnel flow static pressure would yield a total variation in pressure coefficient, from the leading edge pressure gauges to the ones furthest aft, of less than 0.004.

The absence of a data point from a plot indicates that the corresponding gauge either malfunctioned or was covered (for example, by the ventral fin) during the test run. The ordinate scales for the data vary from plot to plot, they were chosen to minimize the number of off-scale points while retaining as much accuracy as possible for the majority of the data points.

REFERENCES

1. Kaufman, L.G. II, et al., A Review of Hypersonic Flow Separation and Control Characteristics, ASD-TDR-62-168, March 1962.

2. Evans, W.J., and Kaufman, L.G. II, Pretest Report on Hypersonic Flow Separation and Control Models for AEDC Tunnels A, B, Hotshot 2 and Grumman Hypersonic Shock Tunnel, Grumman Research Department Memorandum RM-209, July 1962.

3. Hopkins, H.B., Scheuing, R.A., and Leng, J., Investigation of Pressure Distributions over Planar, Twisted, and Cambered Wings in a Hypersonic Shock Tunnel, ASD-TDR-62-171, May 1962.

4. Wallace, A.R., and Swain, W.N., Pressure Distribution Tests on a 60° and 70° Delta Wing at Mach Numbers 20 to 22, AEDC-TN-61-14, February 1961, CONFIDENTIAL REPORT.

5. Kaufman, L.G. II, Pressure and Heat Transfer Measurements for Hypersonic Flows Over Expansion Corners and Ahead of Ramps, ASD-TDR-63-679, Part I: Mach 5 and 8 Data for Expansion Corner Flows, September 1963, Part II: Mach 5 Pressure Data for Flows Ahead of Ramps, September 1963, Part III: Mach 8 Pressure Data for Flows Ahead of Ramps, December 1963, Part IV: Mach 8 Heat Transfer Data for Flows Ahead of Ramps, to be published.

6. Baer, A.L., An Investigation of Separated Flows on Two-Dimensional Models at Mach Numbers 5 and 8, AEDC-TDR-63-200, October 1963.

7. Burchfield, C.G., Hube, F.K., and Burdette, J.E., An Experimental Heat-Transfer Investigation in Regions of Flow Separation at Mach Number 8, AEDC-TDR-64-30, February 1964.

8. Kaufman, L.G. II, Pressure Measurements for Mach 8 Flows Over Expansion Corners and Ramps on an Internally Cooled Model, RTD-TDR-63-4044, Part I: Expansion Corner Flows, October 1963, Part II: Flows Over a Flat Plate with and without a Partial Span Ramp, to be published, Part III: Flows Over Full Span Ramps Mounted on a Flat Plate, to be published.

9. Hartofilis, S.A., Pressure and Heat Transfer Measurements at Mach 13 and 19 for Flows Ahead of Ramps, Over Expansion Corners and Past Fin-Plate Combinations, to be published as an FDL Technical Documentary Report.

10. Kaufman, L.G. II, and Meckler, L.H., Pressure and Heat Transfer Measurements at Mach 5 and 8 for a Fin - Flat Plate Model, ASD-TDR-63-235, April 1963.

11. Kaufman, L.G. II, Pressure Distributions and Oil Film Photographs for Mach 5 Flows Past Fins Mounted on a Flat Plate, ASD-TDR-63-755, September 1963.

12. Kaufman, L.G. II, Pressure Measurements for Mach 5 Flows Over Winged Re-Entry Configurations with Aerodynamic Controls, RTD-TDR-63-4179, Part I: Blunt Cabin Configuration, February 1964, Part II: Conical Cabin Configuration, February 1964.

13. Meckler, L., Pressure Measurements at Mach 8 on an Aerodynamically Controllable Winged Re-Entry Configuration, to be published as an FDL Technical Documentary Report.

14. Meckler, L., Heat Transfer Measurements at Mach 8 on an Aerodynamically Controllable Winged Re-Entry Configuration to be published as an FDL Technical Documentary Report.

15. Donaldson, J.C., Hypersonic Control Effectiveness Tests of a Delta-Winged Re-Entry Configuration at Mach 5 and 8, AEDC-TDR-63-268, December 1963.

16. Hartofilis, S.A., Pressure Measurements at Mach 19 for a Winged Re-Entry Configuration, ASD-TDR-63-319, May 1963.

17. Lacey, J.J. Jr., Pressure Tests on a Blunt Delta Wing Vehicle at M = 19, AEDC-TDR-63-32, February 1963.

18. Meckler, L., Static Aerodynamic Characteristics at Mach 5 and 8 for an Aerodynamically Controllable Winged Re-Entry Configuration, FDL-TDR-64-10, to be published.

19. Kaufman, L.G. II, Pressure Measurements for Mach Five Flows over a Blunt Pyramidal Configuration with Aerodynamic Controls, RTD-TDR-63-4239, January 1964.

20. Kaufman, L.G. II, Pressure and Heat Transfer Measurements for Mach 8 Flows over a Blunt Pyramidal Configuration with Aerodynamic Controls, FDL-TDR-64-2, Part I: Pressure Data for Delta Wing Surface, January 1964, Part II: Pressure Data for Dihedral Surfaces, Part III: Heat Transfer Data for Delta Wing Surface, and Part IV: Heat Transfer Data for Dihedral Surfaces, to be published.

21. Donaldson, J.C., Hypersonic Control Effectiveness Tests of a Blunted, Triangular-Pyramid Re-Entry Configuration at Mach 5 and 8, AEDC-TDR-63-250, December 1963.

22. Evans, W.J. and Kaufman, L.G. II, Aerodynamic Characteristics and Flap Loads for a Blunt Pyramidal Configuration at Mach 5 and 8, to be published as an FDL Technical Documentary Report.

TABLE I

INSTRUMENTATION LOCATIONS

(See also Figure 3)

Instrument No.			X'	Y'	x (feet)
	T	1	0.754	0	
P	R	2	0.887	0	
R	A	3	0.444	-0.449	
E	N	4	0.444	0.449	
S	S	5	0.664	0.433	
S	D	6	0.754	"	
U	U	7	0.887	"	
R	C	8	0.962	"	
E	E	9	0.664	0.472	
	R	10	0.754	"	
	S	11	0.887	"	
		12	0.962	"	
	T	55	0.664	-0.433	0.460
	R G	56	0.754	"	0.523
H	A A	57	0.887	"	0.616
E	N U	58	0.962	"	0.668
A	S G	59	0.664	-0.472	0.460
T	F E	60	0.754	"	0.523
	E S	61	0.887	"	0.616
	R	62	0.962	"	0.668

X' ≡ Nondimensional streamwise distance from virtual apex to planform projection (see Fig. 3).

Y' ≡ Nondimensional spanwise distance outboard from center line (see Fig. 3).

x ≡ streamwise distance from virtual apex to planform projection ($x \equiv [8.325(\text{in})/12(\text{in/ft})] \cdot X'$), used in reducing $\dot{q}_w$ to $Nu/\sqrt{Re_x}$

TABLE II

TEST CONDITIONS

Angle of attack (deg)	Configuration	Figure Numbers (Data plots)	G. H. S. T. run numbers
-30	Basic	7	1470
-30	+ upper flaps	8	1488
-15	Basic	9	1465
-15	+ lower flaps	10	1473
-15	+ upper flaps	11	1485*
0	Basic	12	1460
0	+ lower flaps	13	1471
0	+ upper flaps	14	1484
0	+ ventral fin	15	1461
+14.3**	Basic	16	1464
+14.3	+ lower flaps	17	1475
+14.3	+ upper flaps	18	1483
+14.3	+ ventral fin	19	1463
+30	Basic	20	1466
+30	+ lower flaps	21	1478
+30	+ upper flaps	22	1481
+30	+ ventral fin	23	1467
+45	Basic	24	1468
+45	+ lower flaps	25	1477
+45	+ upper flaps	26	1479
+45	+ ventral fin	27	1469

*Heat transfer data from run 1487.

**Dihedral surfaces parallel to free stream flow at α = +14.3 degrees.

TABLE III

TUNNEL FLOW REFERENCE CONDITIONS*

M_∞	$(p_\infty/p_o)10^6$	$(T_\infty/T_o)10^3$	Essentially constant for all test runs.
20.51	0.1403	13.02	

GHST run number	$p_\infty \times 10^3$ (psia)	q_∞ (psia)	T_∞ (°R)	$k \times 10^6 \left(\frac{BTU}{ft\ sec\ °R}\right)$	$\frac{Re_\infty}{10^3\ ft}$
1460	0.2235	0.06581	47.72	0.4063	71.38
1461	0.2370	0.06979	50.49	0.4298	69.57
1463	0.2353	0.06929	50.12	0.4266	69.82
1464	0.2188	0.06443	46.79	0.3984	71.95
1465	0.2170	0.06390	46.45	0.3956	72.15
1466	0.2029	0.05975	43.81	0.3733	73.63
1467	0.2231	0.06569	47.62	0.4055	71.44
1468	0.1890	0.05565	41.29	0.3519	74.91
1469	0.2112	0.06219	45.34	0.3862	72.79
1470	0.2255	0.06640	48.11	0.4096	71.14
1471	0.2188	0.06443	46.79	0.3984	71.95
1473	0.2150	0.06331	46.05	0.3922	72.38
1475	0.2100	0.06184	45.11	0.3843	72.92
1477	0.2379	0.07005	50.67	0.4313	69.44
1478	0.2344	0.06902	49.93	0.4251	69.95
1479	0.2344	0.06902	49.93	0.4251	69.95
1481	0.2023	0.05957	43.70	0.3723	73.69
1483	0.2270	0.06684	48.40	0.4121	70.95
1484	0.2309	0.06799	49.20	0.4189	70.44
1485	0.2093	0.06163	45.00	**	**
1487	**	0.06350	46.19	0.3934	72.30
1488	0.1795	0.05286	39.62	0.3378	75.69

*Reference conditions at point on tunnel centerline 7.00 inches downstream of nozzle exit.

**Pressure data from run 1485, heat transfer data from run 1487.

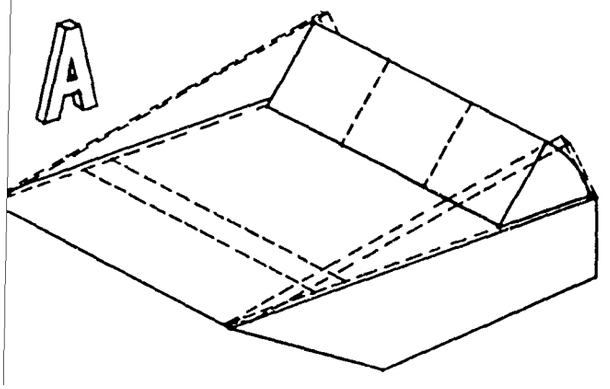

Separated Flows ahead of a Ramp
Fore and aft flaps, end plates
3 separate models:

1) Pressure and heat transfer, AEDC Tunnels A & B, M = 5 & 8, results in Refs. 5-7.

2) Controlled wall temperature, pressure, AEDC Tunnel B, M = 8, results in Refs. 6 and 8.

3) Pressure and heat transfer, Grumman Shock Tunnel, M ≈ 13 & 19, results in Ref. 9.

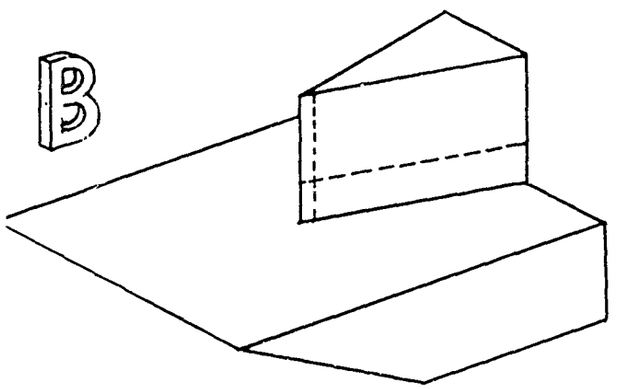

Wedge - Plate Interaction
Small and large fins with sharp and blunt leading edges
2 separate models:

1) Pressure and heat transfer, AEDC Tunnels A & B, M = 5 & 8, results in Refs. 6,7,10 and 11.

2) Pressure and heat transfer, Grumman Shock Tunnel, M ≈ 13 & 19, results in Ref. 9.

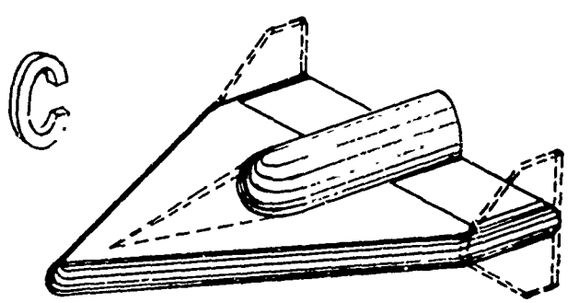

Clipped Delta, Blunt L.E.
Center body, T.E. flaps, drooped nose, spoiler, tip fins
3 separate models:

1) Pressure and heat transfer, AEDC Tunnels A & B, M = 5 & 8, results in Refs. 7 and 12-15.

2) Pressure, AEDC Hotshop 2, M ≈ 19, results in Refs. 16 and 17.

3) Six component force, AEDC Tunnels A & B, M = 5 & 8, results in Refs. 15 and 18.

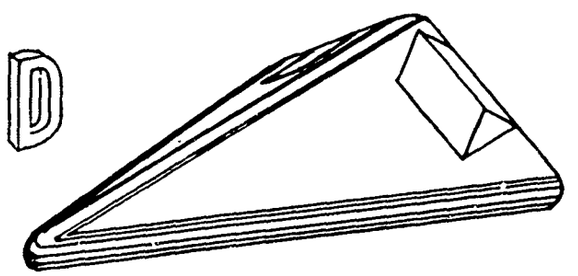

Delta, Blunt L.E., Dihedral
T.E. flaps, canard, ventral fin
3 separate models:

1) Pressure and heat transfer, AEDC Tunnels A & B, M = 5 & 8, results in Refs. 7 and 19-21.

2) Pressure and heat transfer, Grumman Shock Tunnel, M ≈ 19, results herein.

3) Six component force, AEDC Tunnels A & B, M = 5 & 8, results in Refs. 21 and 22.

Fig. 1 General Outline of Models and Remarks for Over-all Program

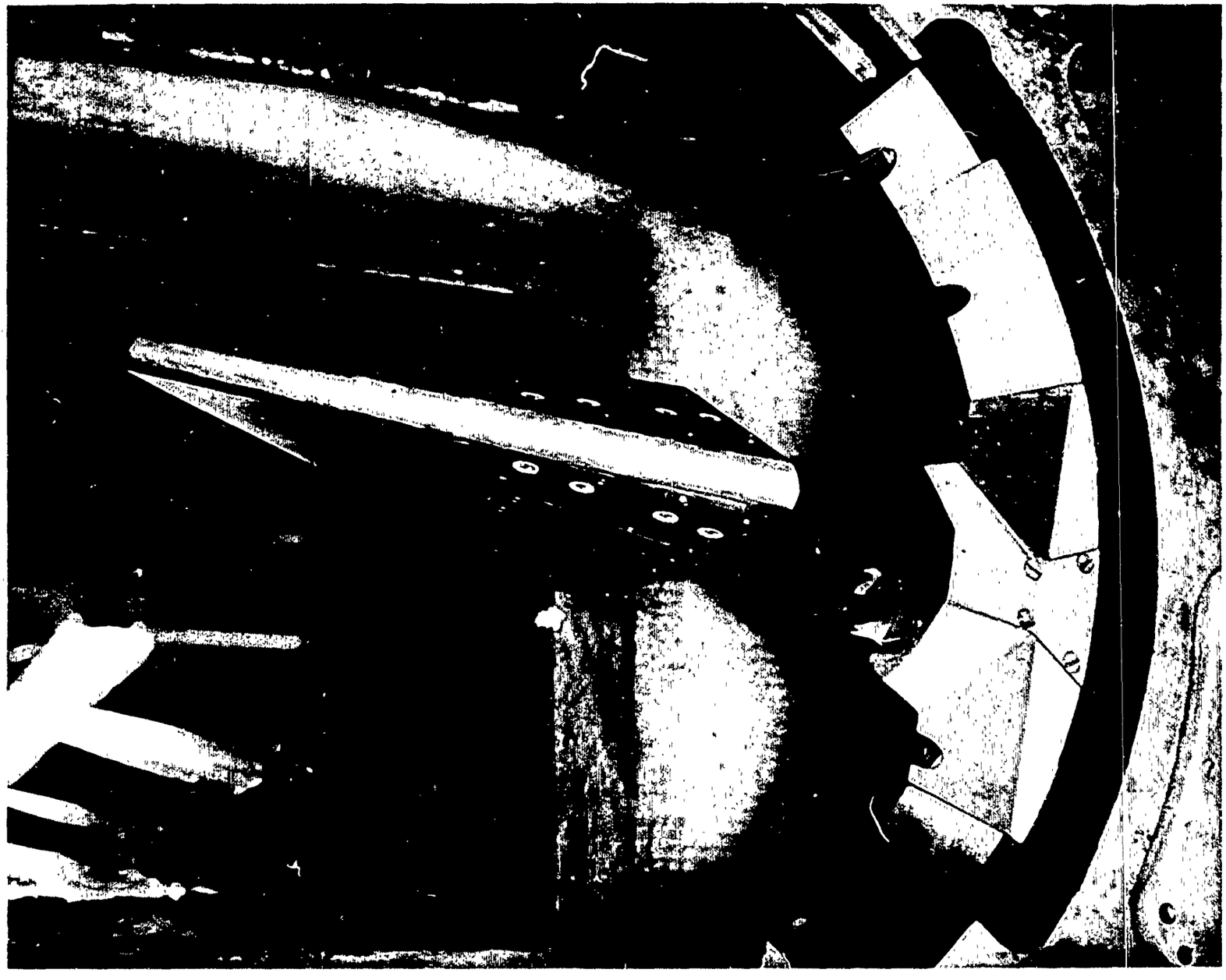

Fig. 2 Photograph of Model Installed in the Grumman Hypersonic Shock Tunnel

Fig. 3 Photograph of Model with Upper Surface Flaps Attached

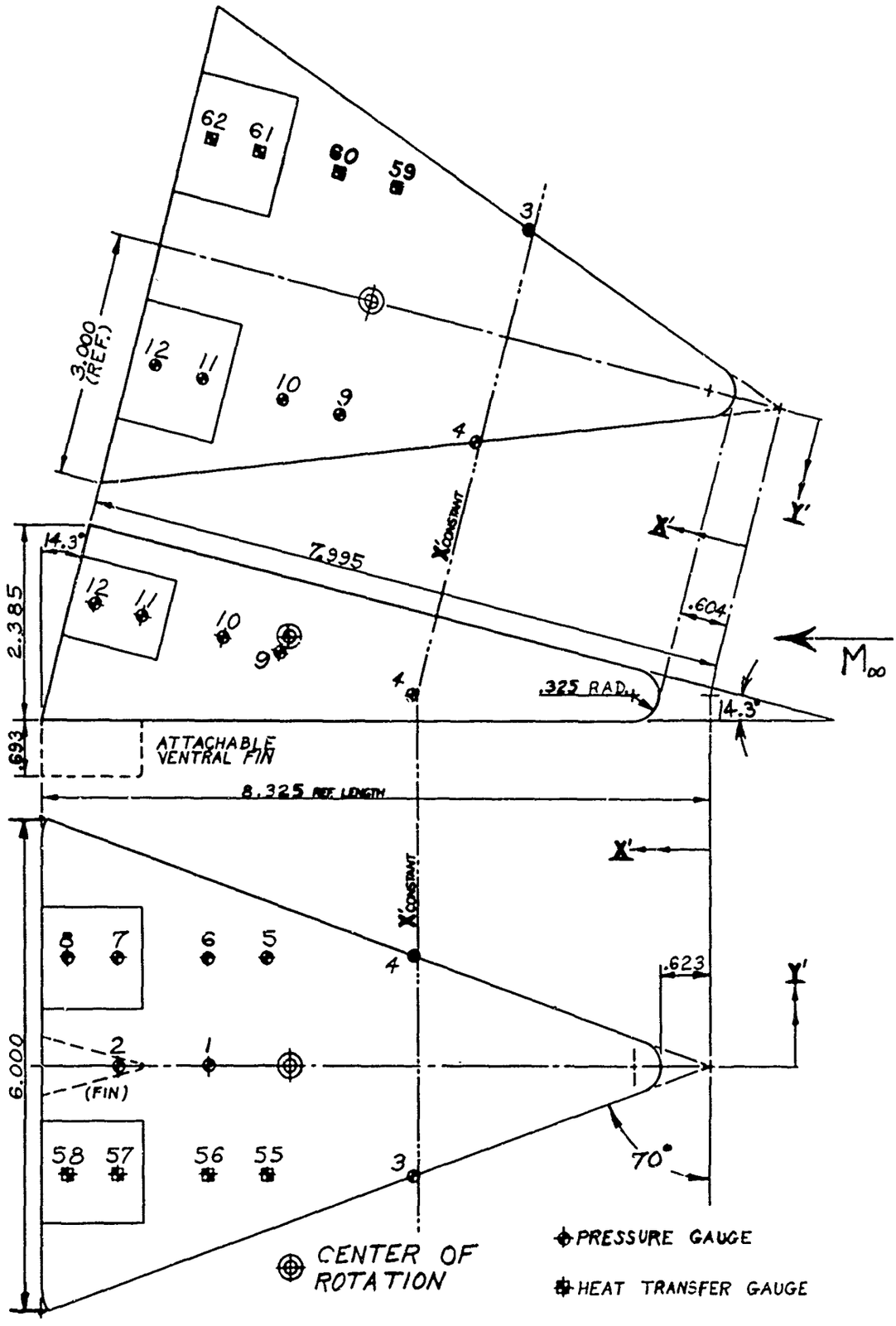

Fig. 4 Model Instrumentation

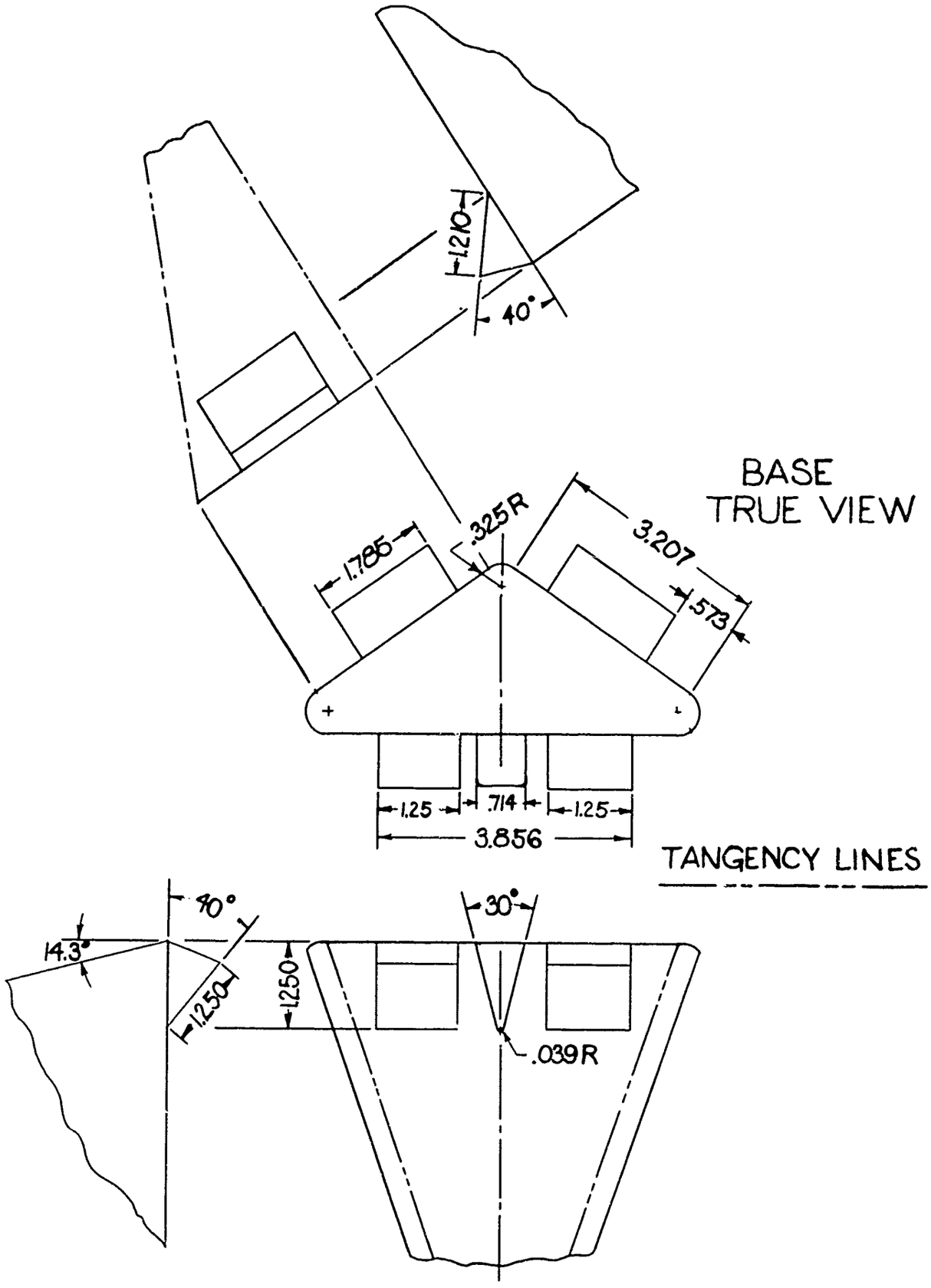

Fig. 5 Flap and Fin Geometry

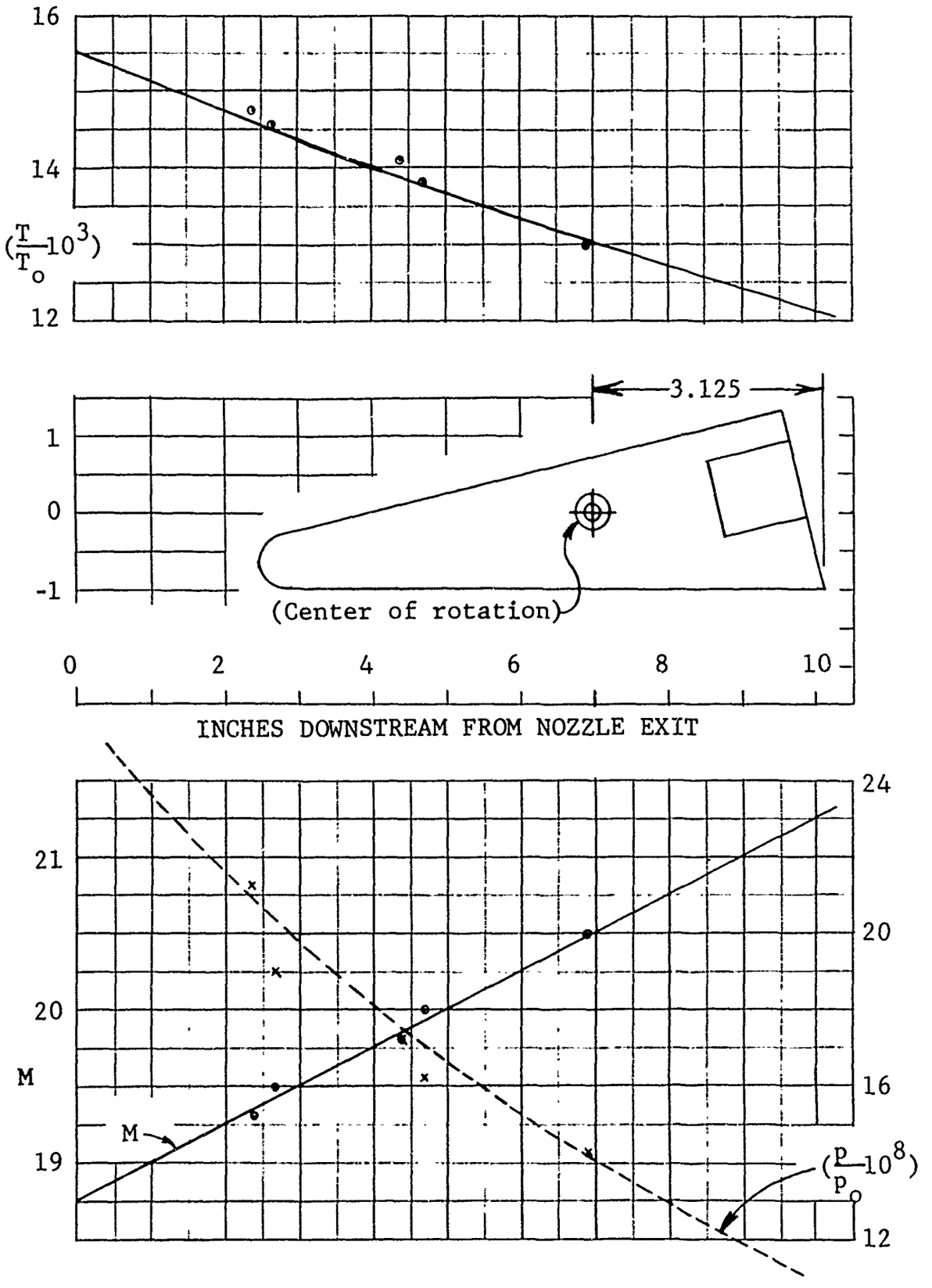

Fig. 6 Tunnel Centerline Distributions of Mach Number and Static to Total Pressure and Temperature Ratios

Symbols	Gauge numbers and locations		
×	1 and 2	(lower surface),	Y' = 0
◈	3	(leading edge),	Y' = -0.449
⊡	4	(leading edge),	Y' = 0.449
⊙	5 thru 8	(lower surface),	Y' = 0.433
▶	9 thru 12	(upper surface),	Y' = 0.472
●	55 thru 58	(lower surface),	Y' = -0.433
▶	59 thru 62	(upper surface),	Y' = -0.472

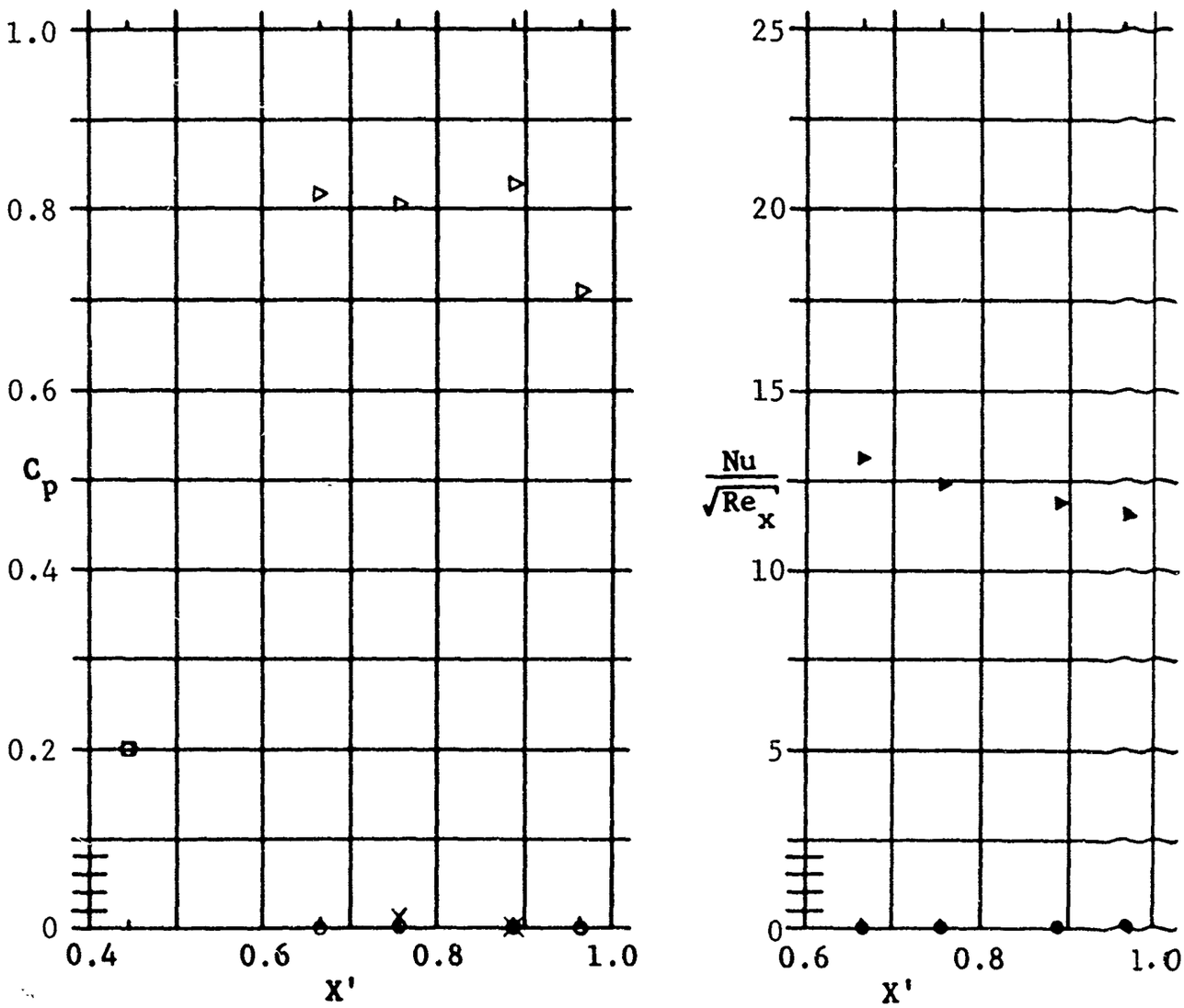

Fig. 7 C_p and $Nu/\sqrt{Re_x}$ versus X' for Basic Configuration at $\alpha = -30°$

Symbols	Gauge numbers and locations		
×	1 and 2	(lower surface),	Y' = 0
◈	3	(leading edge),	Y' = -0.449
⊡	4	(leading edge),	Y' = 0.449
⊙	5 thru 8	(lower surface),	Y' = 0.433
▷	9 thru 12	(upper surface),	Y' = 0.472
●	55 thru 58	(lower surface),	Y' = -0.433
▶	59 thru 62	(upper surface),	Y' = -0.472

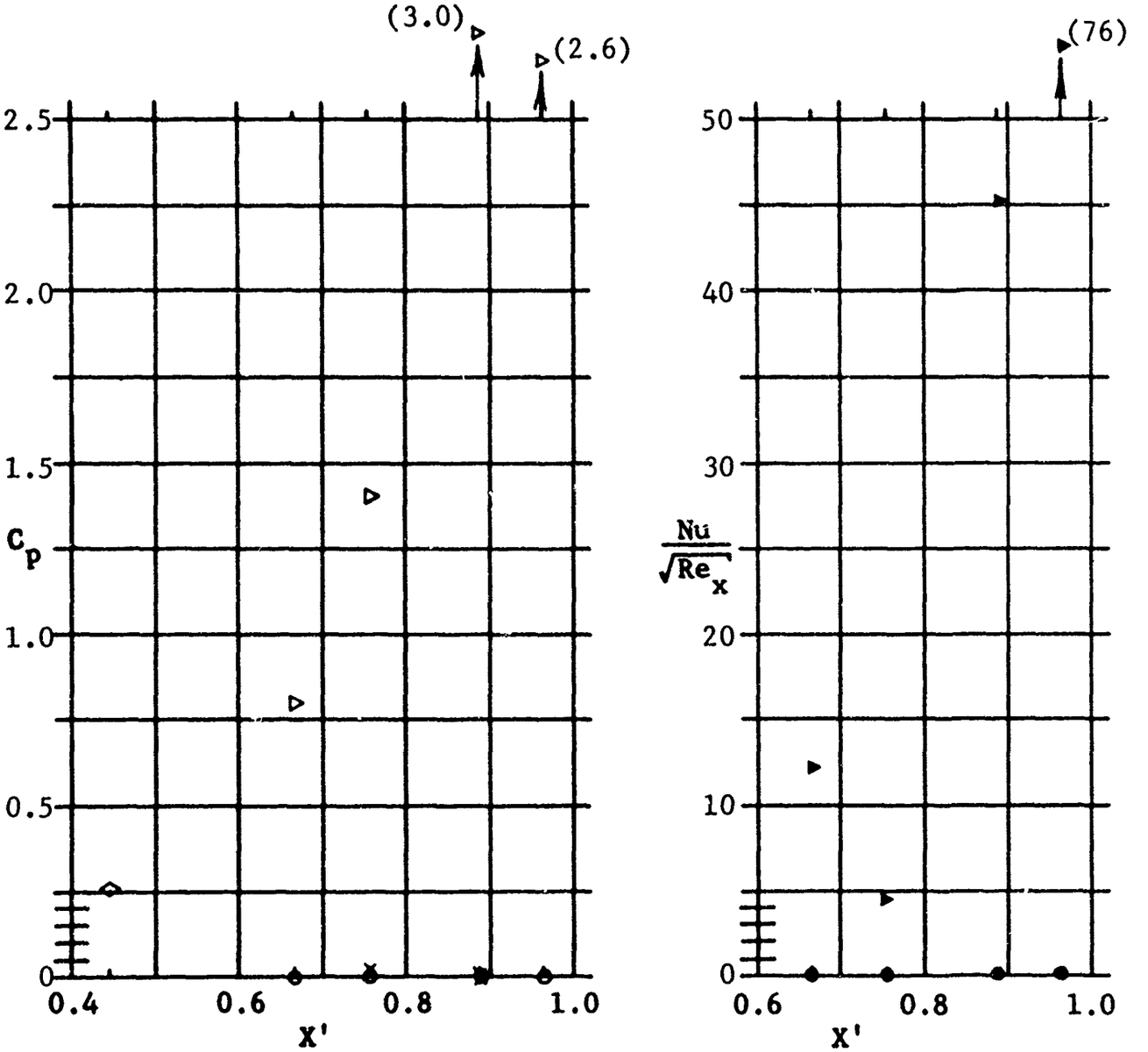

Fig. 8 C_p and $Nu/\sqrt{Re_x}$ versus X' for Basic Configuration with Upper (Dihedral) Surface Flaps at $\alpha = -30°$

Symbols	Gauge numbers and locations		
×	1 and 2	(lower surface),	Y' = 0
◈	3	(leading edge),	Y' = -0.449
⊡	4	(leading edge),	Y' = 0.449
⊙	5 thru 8	(lower surface),	Y' = 0.433
▷	9 thru 12	(upper surface),	Y' = 0.472
●	55 thru 58	(lower surface),	Y' = -0.433
▶	59 thru 62	(upper surface),	Y' = -0.472

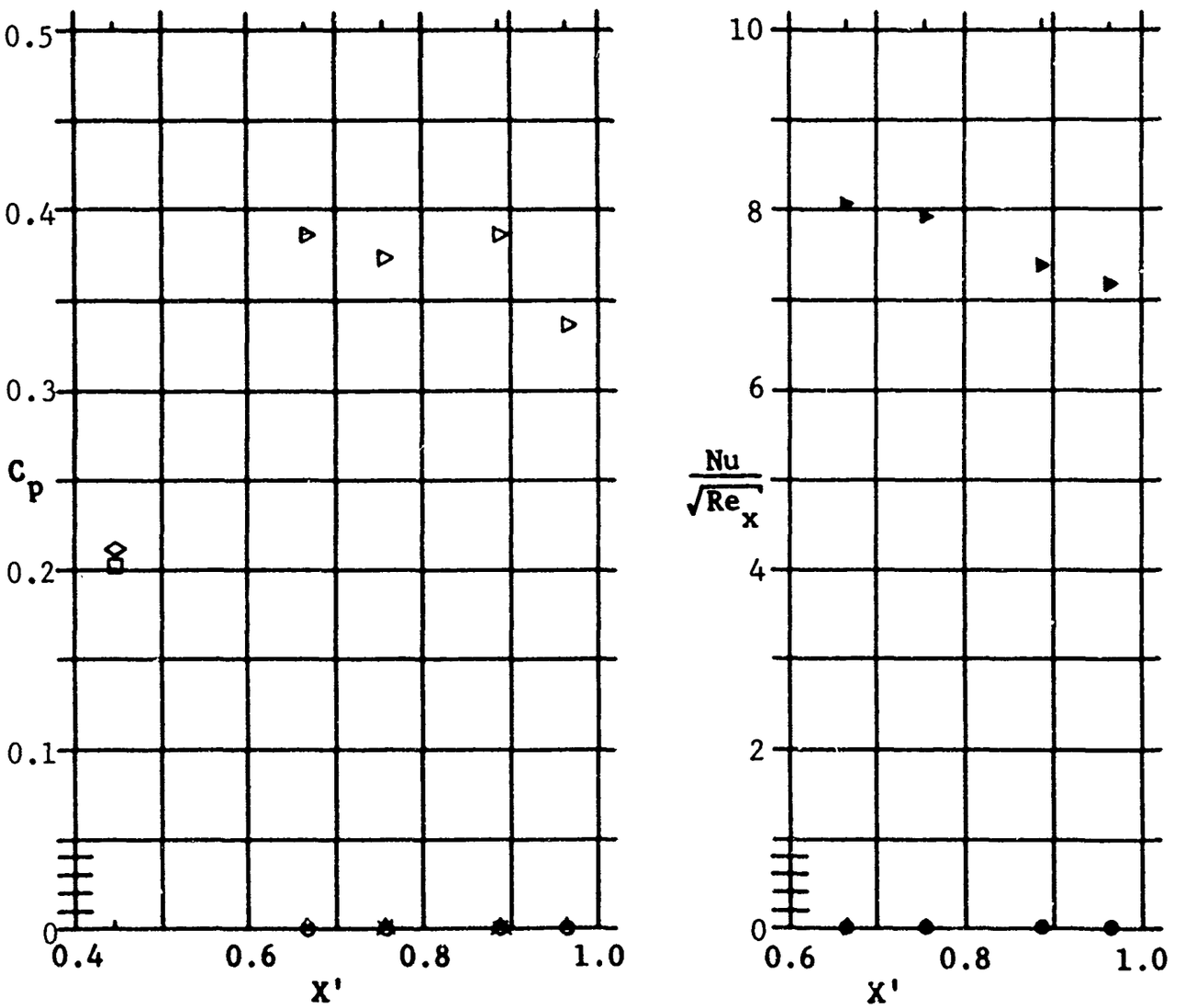

Fig. 9 C_p and $Nu/\sqrt{Re_x}$ versus X' for Basic Configuration at $\alpha = -15°$

Symbols	Gauge numbers and locations		
×	1 and 2	(lower surface),	Y' = 0
◈	3	(leading edge),	Y' = -0.449
⊡	4	(leading edge),	Y' = 0.449
⊙	5 thru 8	(lower surface),	Y' = 0.433
▷	9 thru 12	(upper surface),	Y' = 0.472
●	55 thru 58	(lower surface),	Y' = -0.433
▶	59 thru 62	(upper surface),	Y' = -0.472

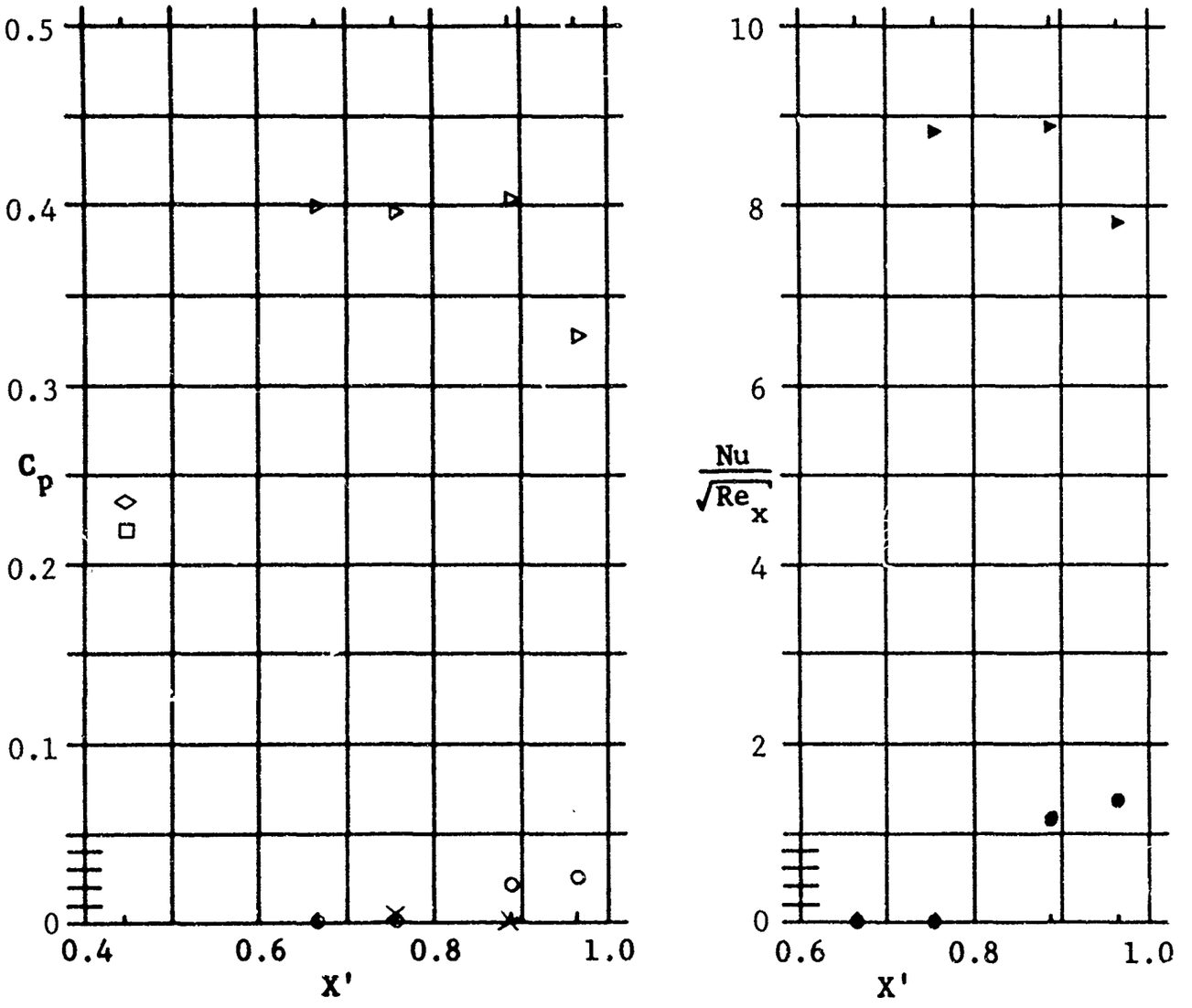

Fig. 10 C_p and $Nu/\sqrt{Re_x}$ versus X' for Basic Configuration with Lower Surface Flaps at α = - 15°

Symbols	Gauge numbers and locations		
×	1 and 2	(lower surface),	Y' = 0
◈	3	(leading edge),	Y' = -0.449
⊡	4	(leading edge),	Y' = 0.449
⊙	5 thru 8	(lower surface),	Y' = 0.433
▶	9 thru 12	(upper surface),	Y' = 0.472
●	55 thru 58	(lower surface),	Y' = -0.433
▶	59 thru 62	(upper surface),	Y' = -0.472

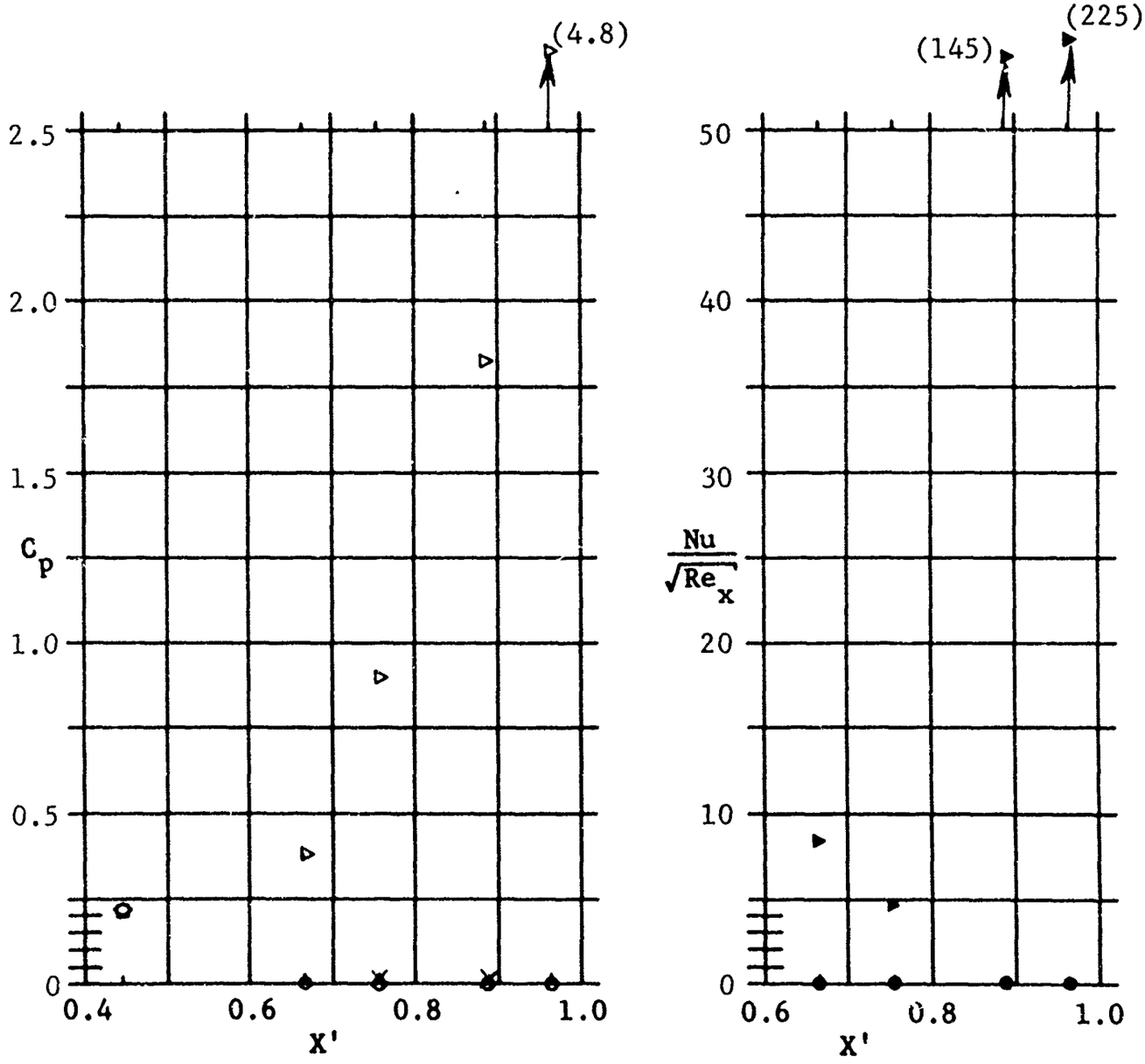

Fig. 11 C_p and $Nu/\sqrt{Re_x}$ versus X' for Basic Configuration with Upper (Dihedral) Surface Flaps at $\alpha = -15°$

Symbols	Gauge numbers and locations		
×	1 and 2	(lower surface),	Y' = 0
◈	3	(leading edge),	Y' = -0.449
⊡	4	(leading edge),	Y' = 0.449
⊙	5 thru 8	(lower surface),	Y' = 0.433
▶	9 thru 12	(upper surface),	Y' = 0.472
●	55 thru 58	(lower surface),	Y' = -0.433
▶	59 thru 62	(upper surface),	Y' = -0.472

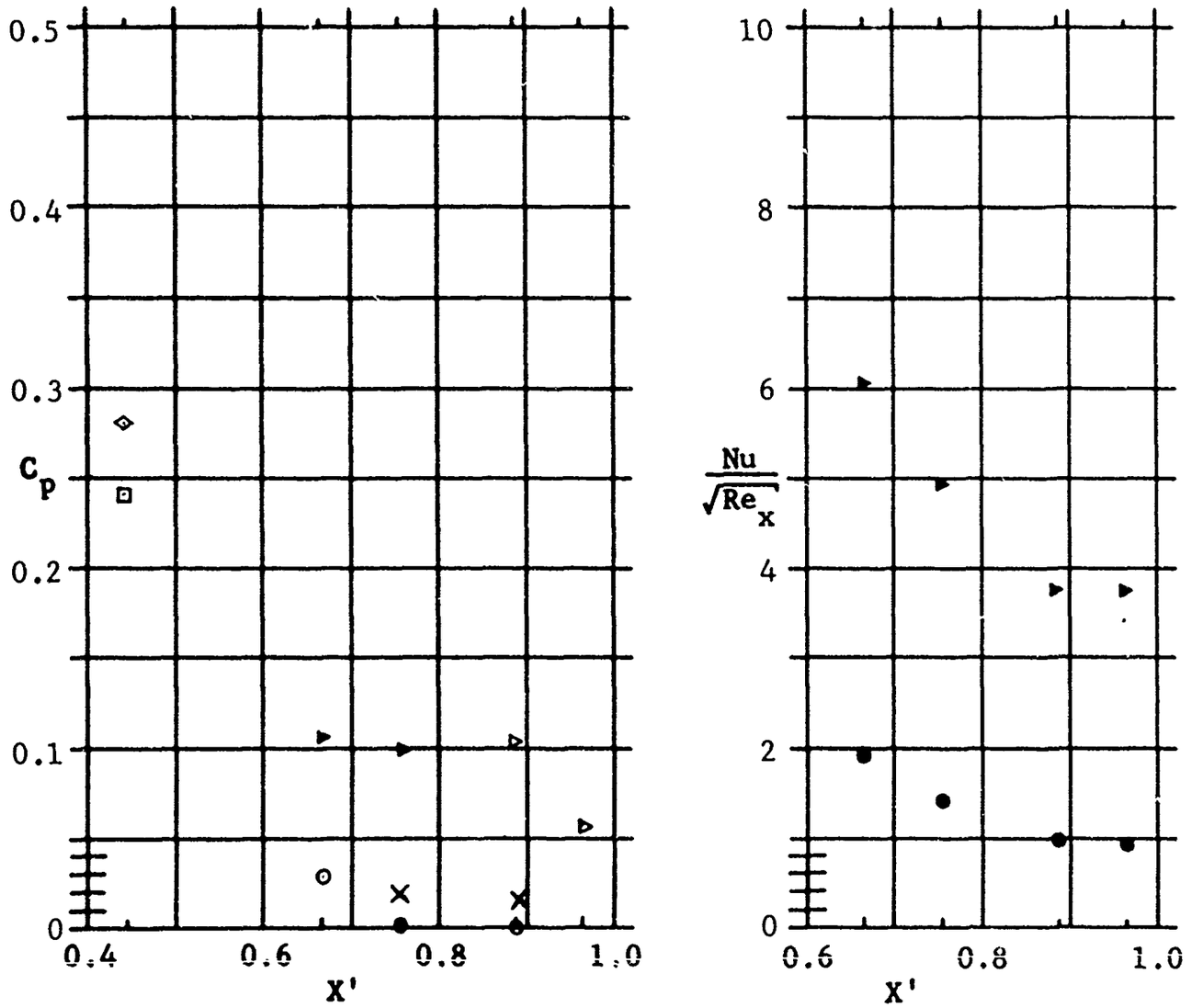

Fig. 12 C_p and $Nu/\sqrt{Re_x}$ versus X' for Basic Configuration at $\alpha = 0$

Symbols	Gauge numbers and locations		
×	1 and 2	(lower surface),	Y' = 0
◈	3	(leading edge),	Y' = -0.449
⊡	4	(leading edge),	Y' = 0.449
⊙	5 thru 8	(lower surface),	Y' = 0.433
▶	9 thru 12	(upper surface),	Y' = 0.472
●	55 thru 58	(lower surface),	Y' = -0.433
▶	59 thru 62	(upper surface),	Y' = -0.472

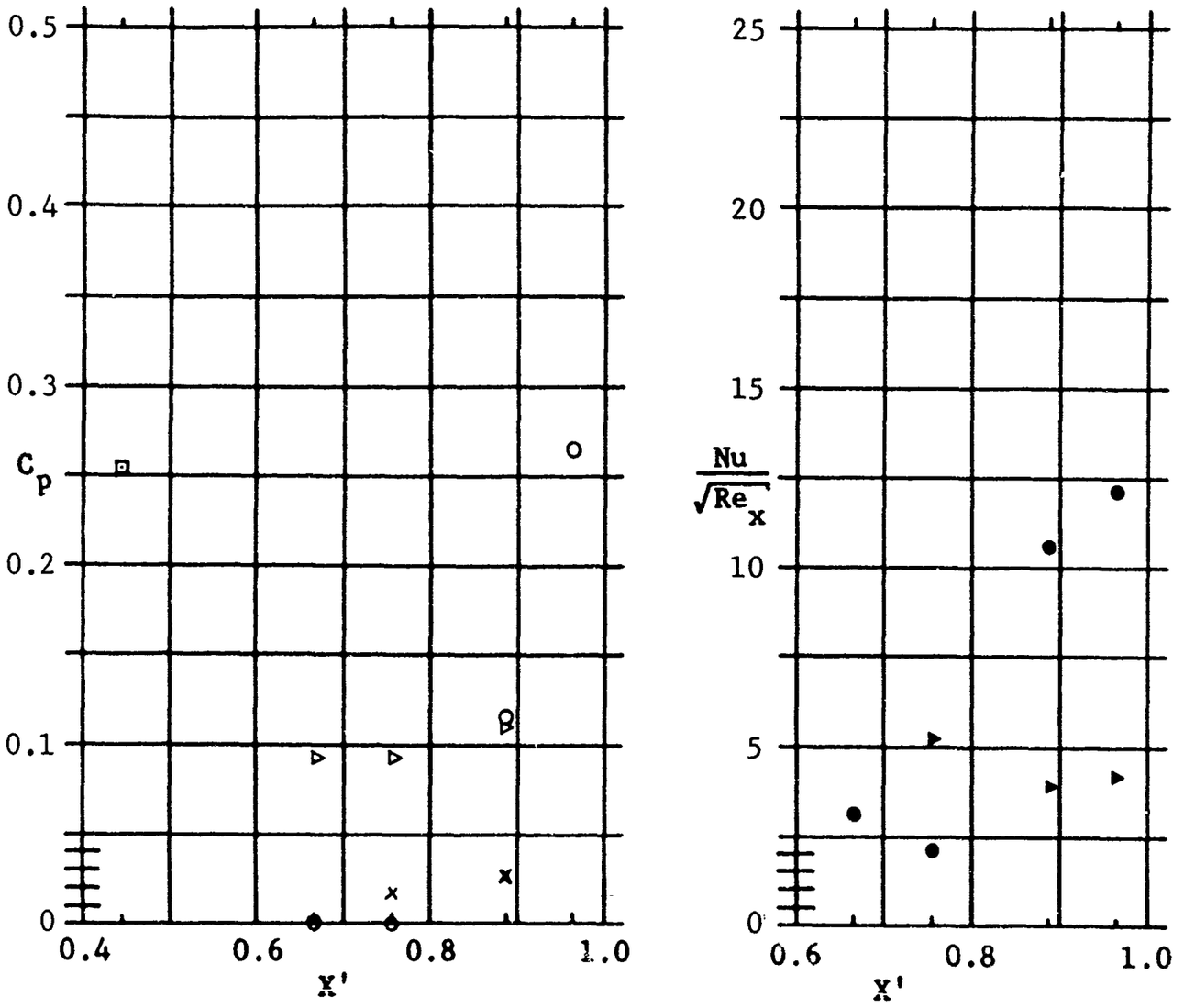

Fig. 13 C_p and $Nu/\sqrt{Re_x}$ versus X' for Basic Configuration with Lower Surface Flaps at $\alpha = 0$

Symbols	Gauge numbers and locations		
×	1 and 2	(lower surface),	Y' = 0
◈	3	(leading edge),	Y' = -0.449
⊡	4	(leading edge),	Y' = 0.449
⊙	5 thru 8	(lower surface),	Y' = 0.433
▶	9 thru 12	(upper surface),	Y' = 0.472
●	55 thru 58	(lower surface),	Y' = -0.433
▶	59 thru 62	(upper surface),	Y' = -0.472

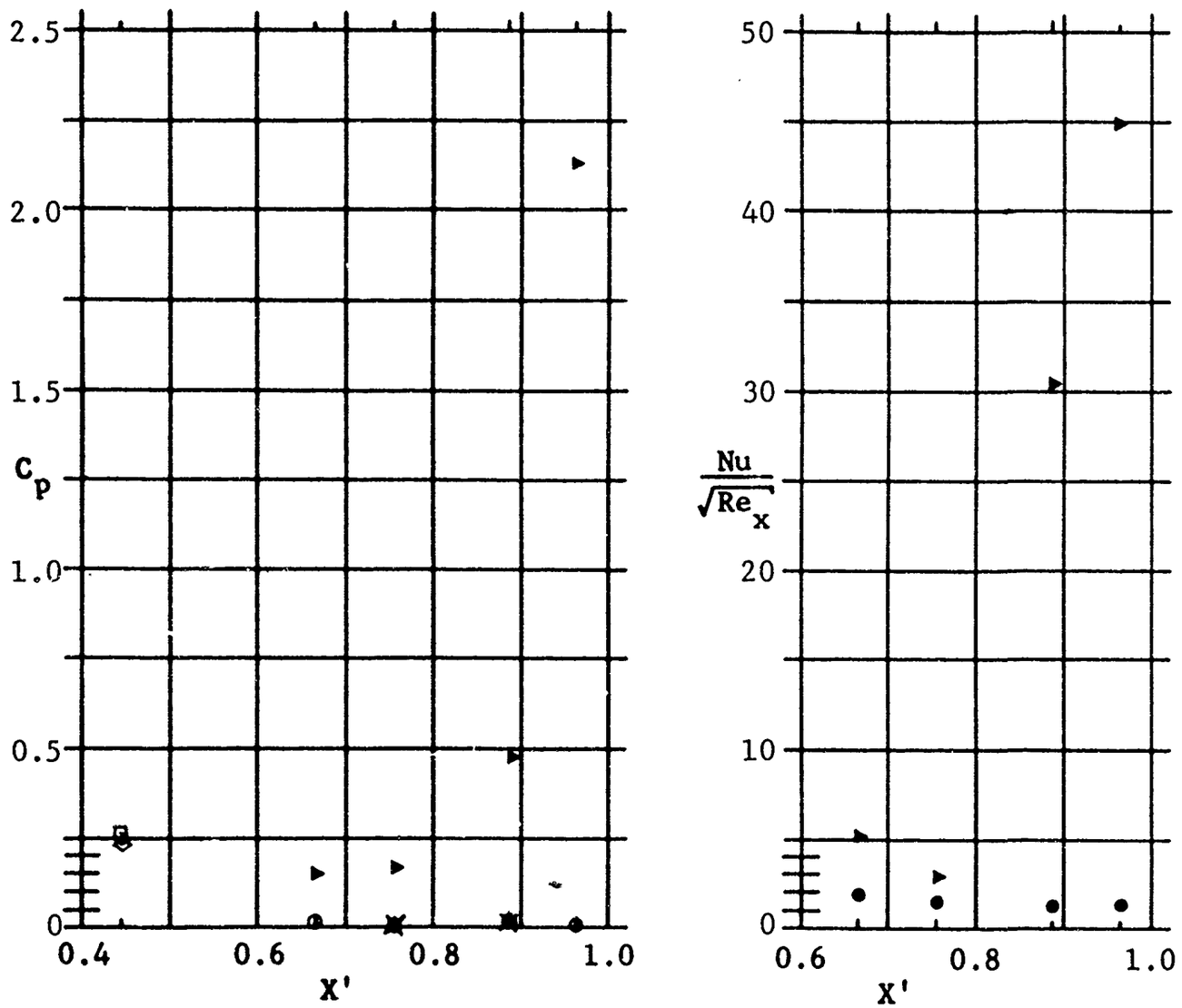

Fig. 14 C_p and $Nu/\sqrt{Re_x}$ versus X' for Basic Configuration with Upper (Dihedral) Surface Flaps at $\alpha = 0$

Symbols	Gauge numbers and locations	
×	1 and 2	(lower surface), Y' = 0
◈	3	(leading edge), Y' = -0.449
⊡	4	(leading edge), Y' = 0.449
⊙	5 thru 8	(lower surface), Y' = 0.433
▶	9 thru 12	(upper surface), Y' = 0.472
●	55 thru 58	(lower surface), Y' = -0.433
▶	59 thru 62	(upper surface), Y' = -0.472

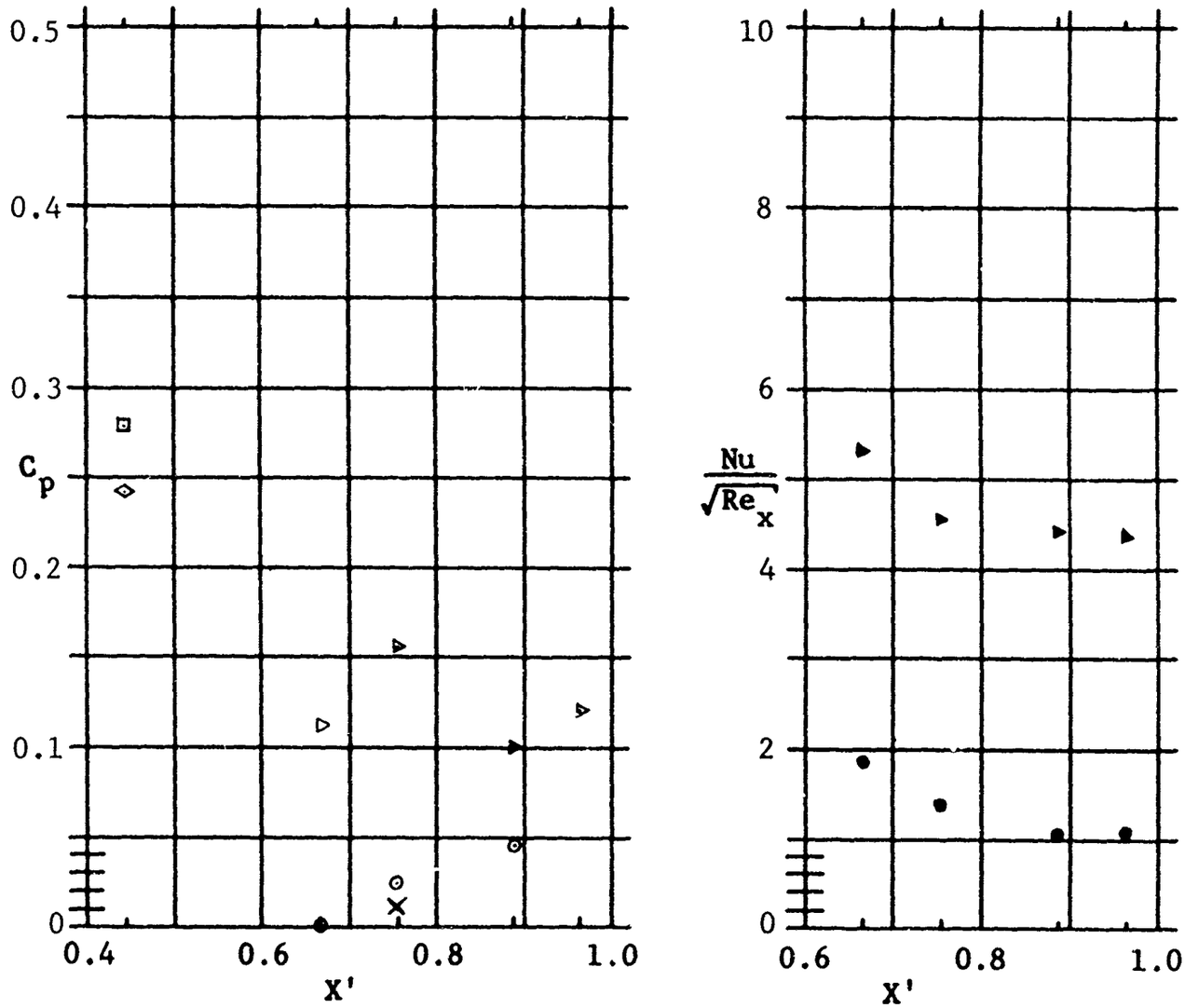

Fig. 15 C_p and $Nu/\sqrt{Re_x}$ versus X' for Basic Configuration with Ventral Fin at $\alpha = 0$

Symbols	Gauge numbers and locations		
×	1 and 2	(lower surface),	Y' = 0
◈	3	(leading edge),	Y' = -0.449
⊡	4	(leading edge),	Y' = 0.449
⊙	5 thru 8	(lower surface),	Y' = 0.433
▶	9 thru 12	(upper surface),	Y' = 0.472
●	55 thru 58	(lower surface),	Y' = -0.433
▶	59 thru 62	(upper surface),	Y' = -0.472

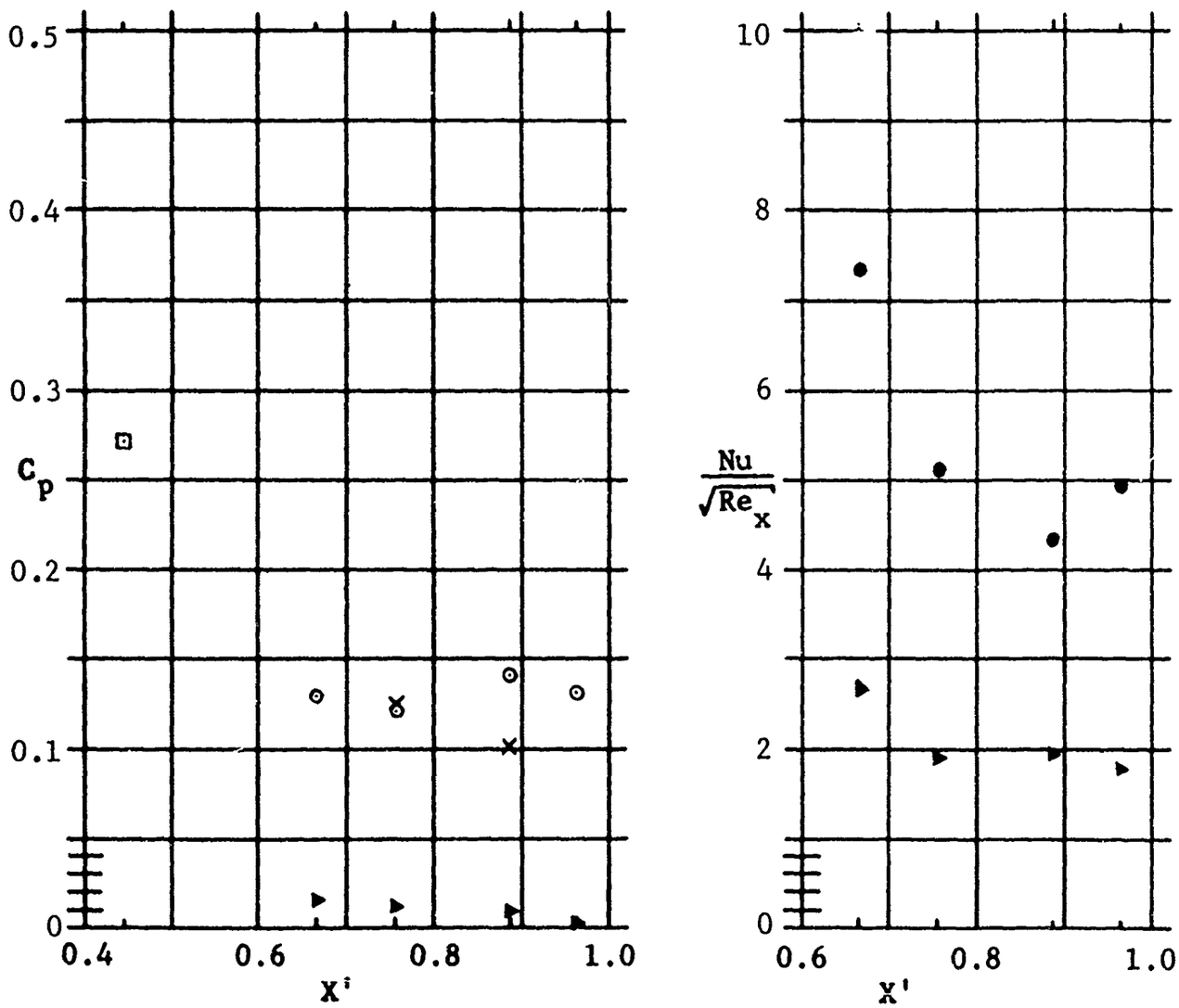

Fig. 16 C_p and $Nu/\sqrt{Re_x}$ versus X' for Basic Configuration at $\alpha = +14.3°$

Symbols	Gauge numbers and locations		
×	1 and 2	(lower surface),	Y' = 0
◈	3	(leading edge),	Y' = -0.449
⊡	4	(leading edge),	Y' = 0.449
⊙	5 thru 8	(lower surface),	Y' = 0.433
▶	9 thru 12	(upper surface),	Y' = 0.472
●	55 thru 58	(lower surface),	Y' = -0.433
▶	59 thru 62	(upper surface),	Y' = -0.472

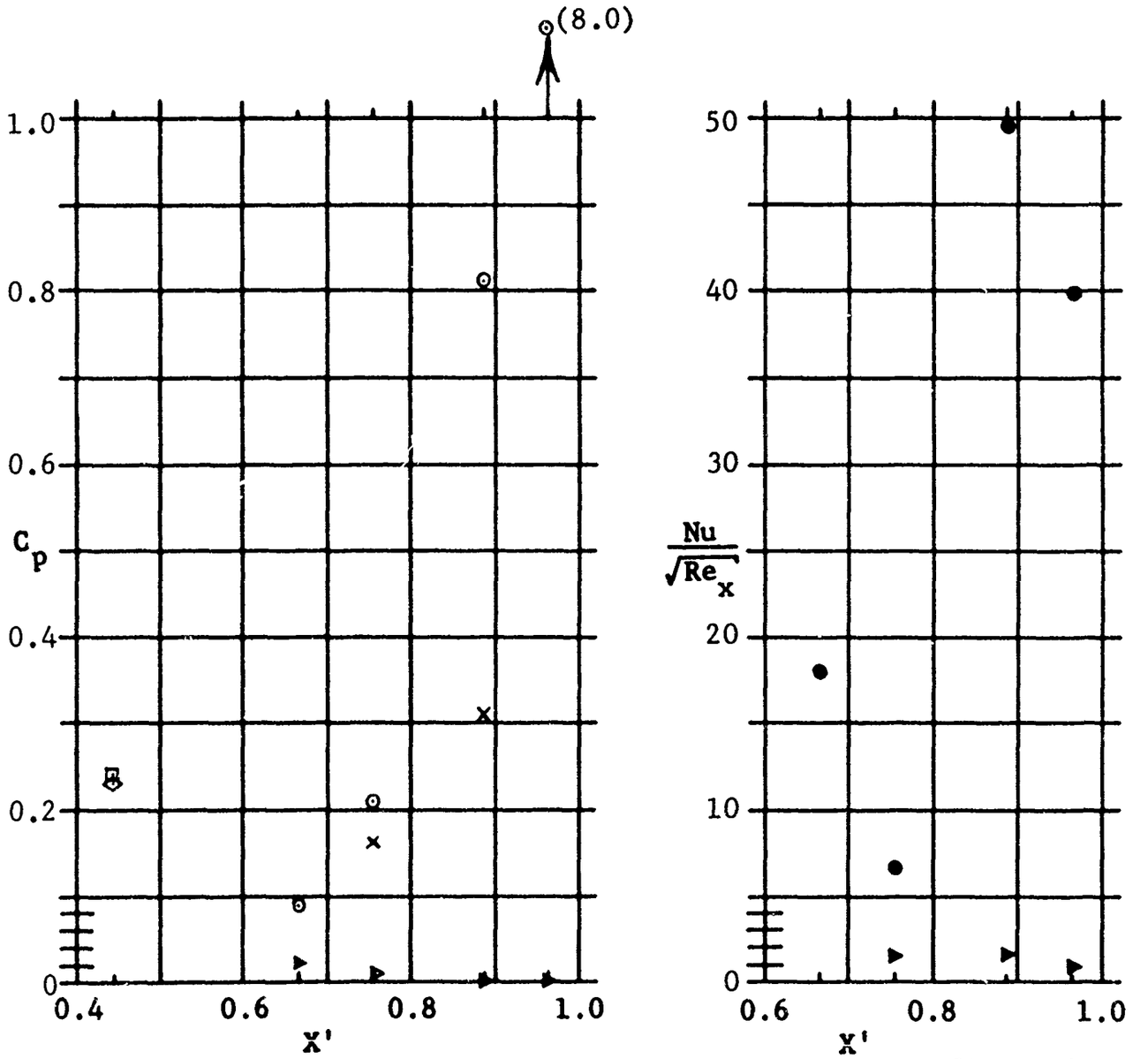

Fig. 17 C_p and $Nu/\sqrt{Re_x}$ versus X' for Basic Configuration with Lower Surface Flaps at $\alpha = +14.3°$

Symbols	Gauge numbers and locations		
×	1 and 2	(lower surface),	Y' = 0
◈	3	(leading edge),	Y' = -0.449
⊡	4	(leading edge),	Y' = 0.449
⊙	5 thru 8	(lower surface),	Y' = 0.433
▶	9 thru 12	(upper surface),	Y' = 0.472
●	55 thru 58	(lower surface),	Y' = -0.433
▶	59 thru 62	(upper surface),	Y' = -0.472

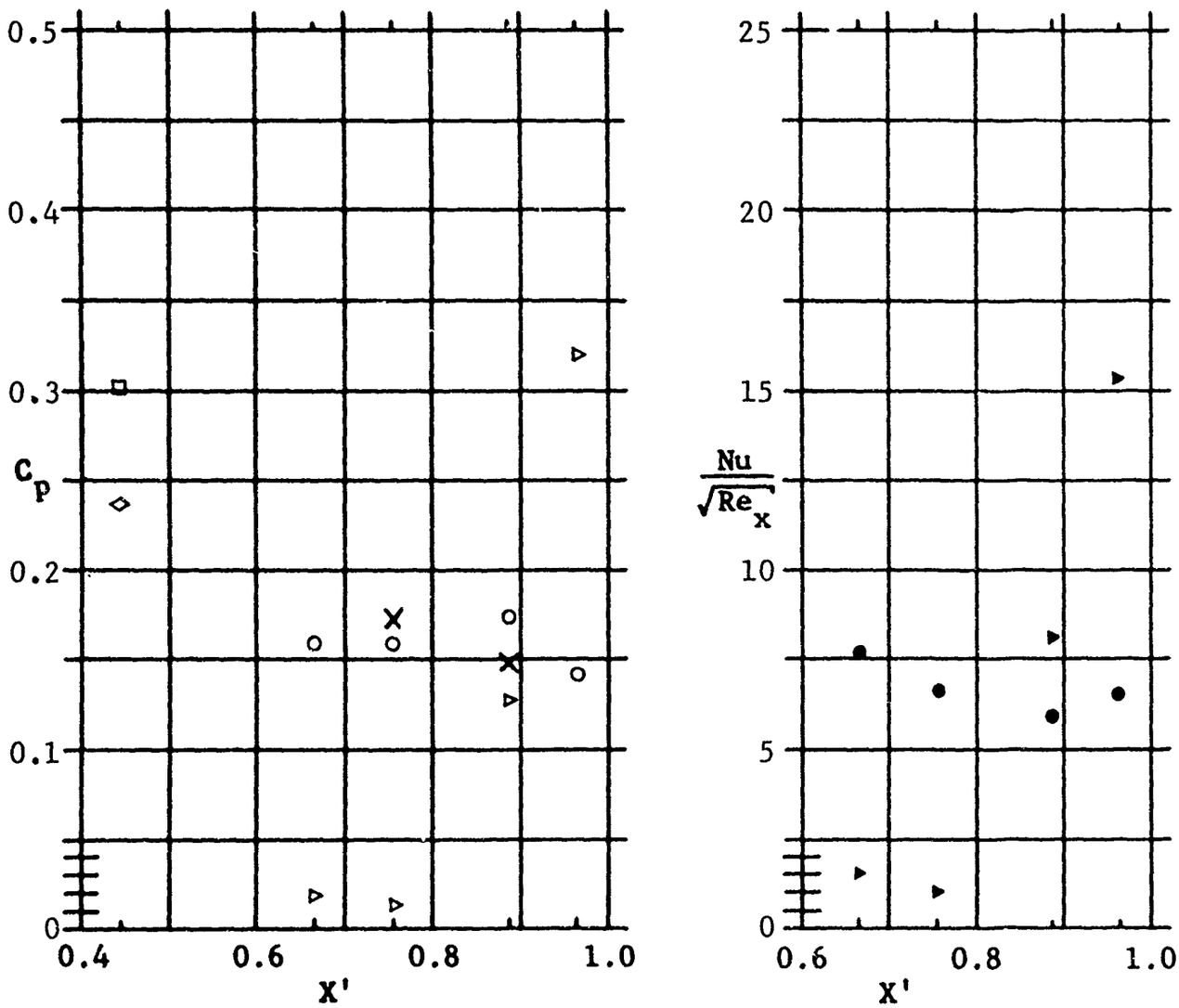

Fig. 18 C_p and $Nu/\sqrt{Re_x}$ versus X' for Basic Configuration with Upper (Dihedral) Surface Flaps at $\alpha = +14.3°$

Symbols	Gauge numbers and locations		
×	1 and 2	(lower surface),	Y' = 0
◈	3	(leading edge),	Y' = -0.449
⊡	4	(leading edge),	Y' = 0.449
⊙	5 thru 8	(lower surface),	Y' = 0.433
▶	9 thru 12	(upper surface),	Y' = 0.472
●	55 thru 58	(lower surface),	Y' = -0.433
▶	59 thru 62	(upper surface),	Y' = -0.472

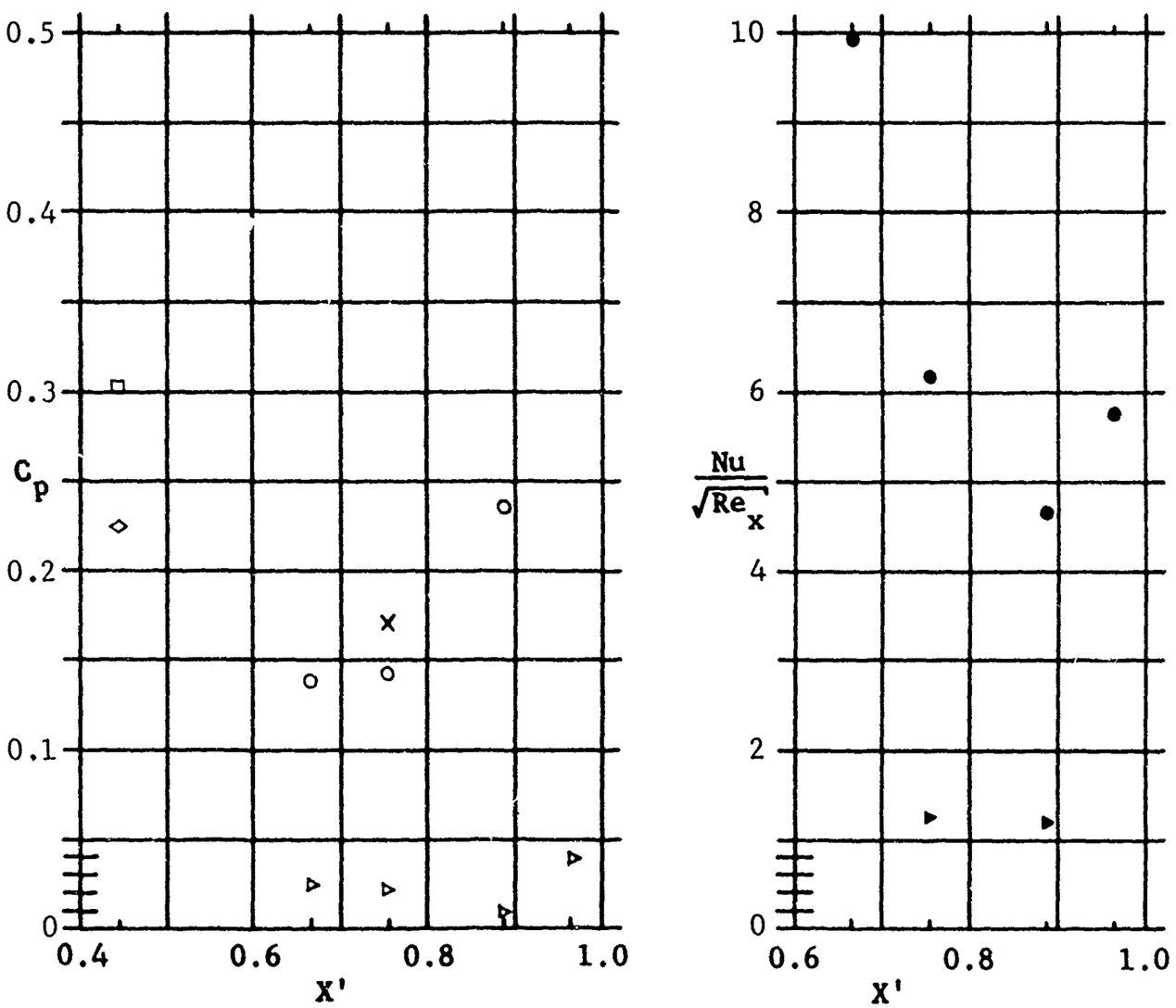

Fig. 19 C_p and $Nu/\sqrt{Re_x}$ versus X' for Basic Configuration with Ventral Fin at $\alpha = +14.3°$

Symbols	Gauge numbers and locations		
×	1 and 2	(lower surface),	Y' = 0
◈	3	(leading edge),	Y' = -0.449
⊡	4	(leading edge),	Y' = 0.449
⊙	5 thru 8	(lower surface),	Y' = 0.433
▶	9 thru 12	(upper surface),	Y' = 0.472
●	55 thru 58	(lower surface),	Y' = -0.433
▶	59 thru 62	(upper surface),	Y' = -0.472

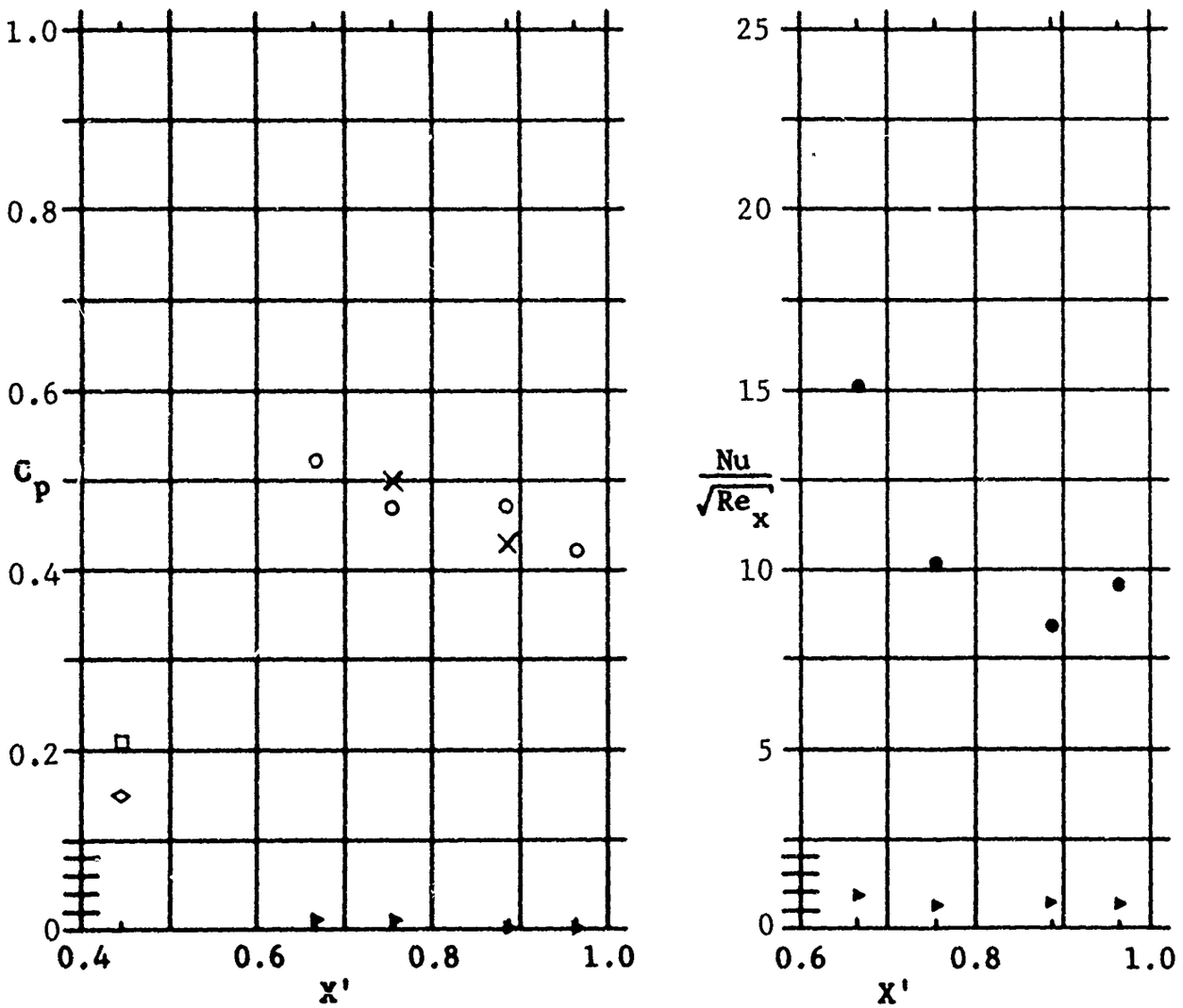

Fig. 20 C_p and $Nu/\sqrt{Re_x}$ versus X' for Basic Configuration at $\alpha = +30°$

Symbols	Gauge numbers and locations		
×	1 and 2	(lower surface),	Y' = 0
◈	3	(leading edge),	Y' = -0.449
⊡	4	(leading edge),	Y' = 0.449
◉	5 thru 8	(lower surface),	Y' = 0.433
▶	9 thru 12	(upper surface),	Y' = 0.472
●	55 thru 58	(lower surface),	Y' = -0.433
▶	59 thru 62	(upper surface),	Y' = -0.472

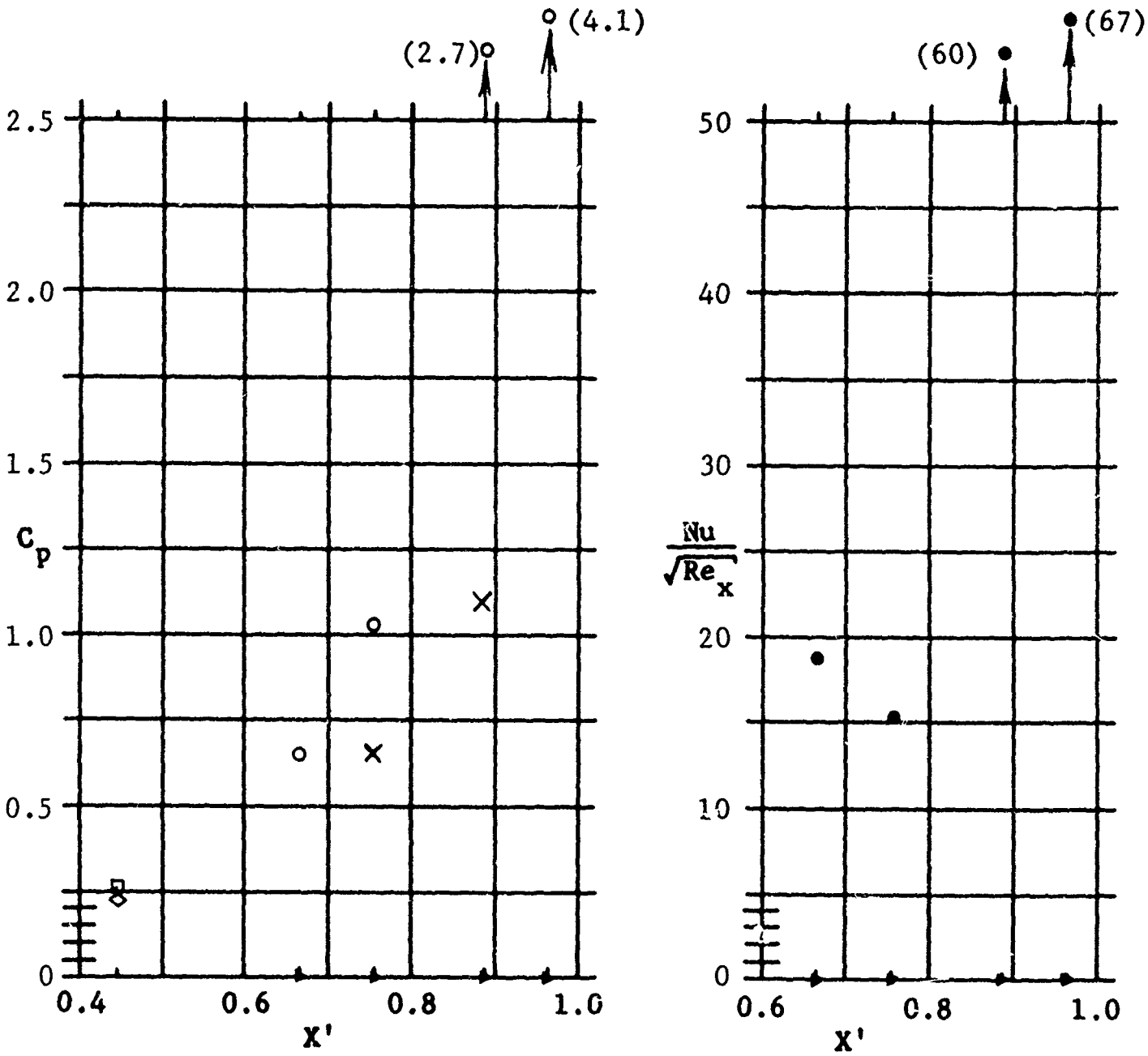

Fig. 21 C_p and $Nu/\sqrt{Re_x}$ versus X' for Basic Configuration with Lower Surface Flaps at $\alpha = +30°$

Symbols	Gauge numbers and locations		
×	1 and 2	(lower surface),	Y' = 0
◆	3	(leading edge),	Y' = -0.449
⊡	4	(leading edge),	Y' = 0.449
⊙	5 thru 8	(lower surface),	Y' = 0.433
▶	9 thru 12	(upper surface),	Y' = 0.472
●	55 thru 58	(lower surface),	Y' = -0.433
▶	59 thru 62	(upper surface),	Y' = -0.472

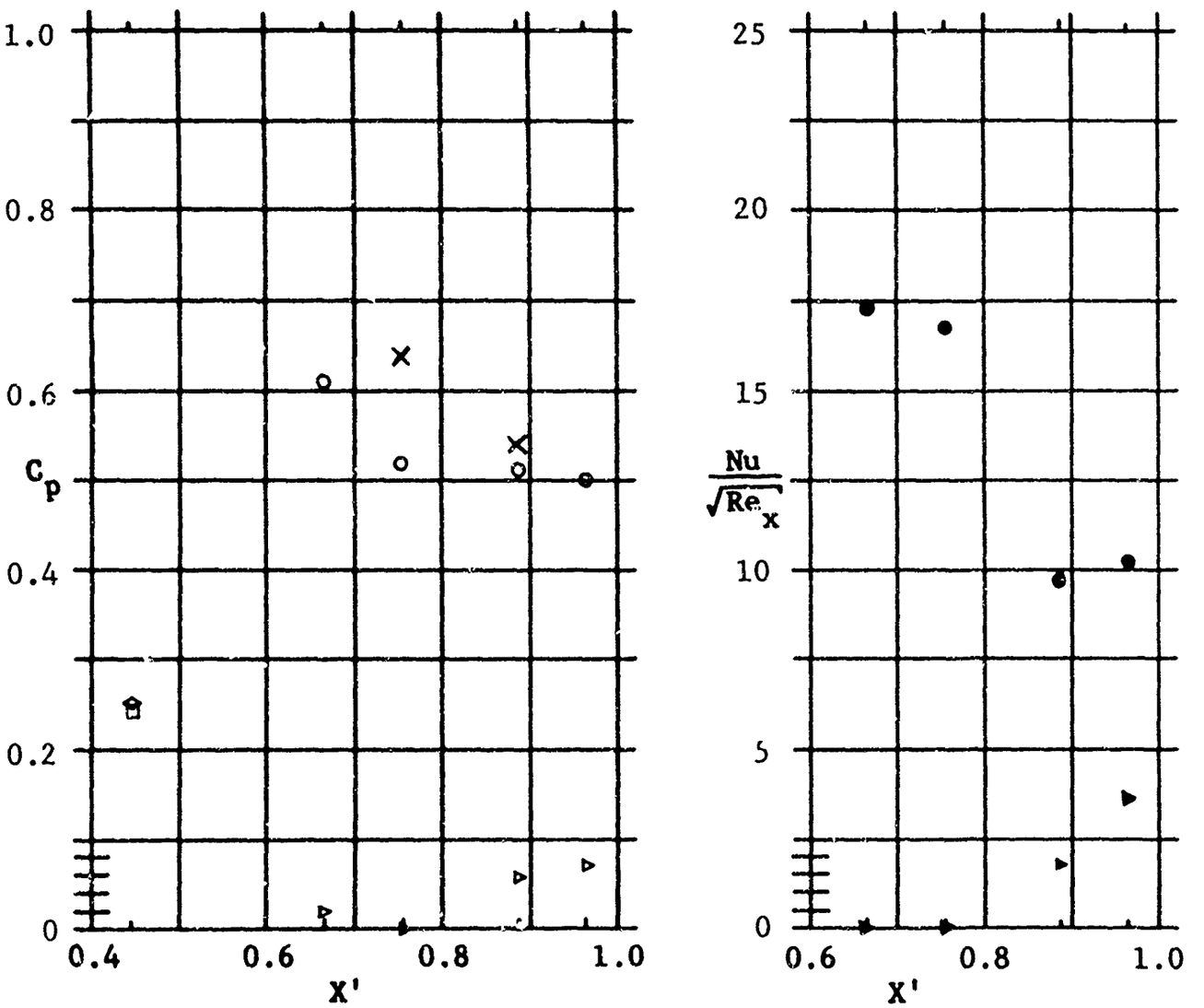

Fig. 22 C_p and $Nu/\sqrt{Re_x}$ versus X' for Basic Configuration with Upper (Dihedral) Surface Flaps at $\alpha = +30°$

Symbols	Gauge numbers and locations	
×	1 and 2	(lower surface), Y' = 0
◈	3	(leading edge), Y' = -0.449
⊡	4	(leading edge), Y' = 0.449
⊙	5 thru 8	(lower surface), Y' = 0.433
▶	9 thru 12	(upper surface), Y' = 0.472
●	55 thru 58	(lower surface), Y' = -0.433
▶	59 thru 62	(upper surface), Y' = -0.472

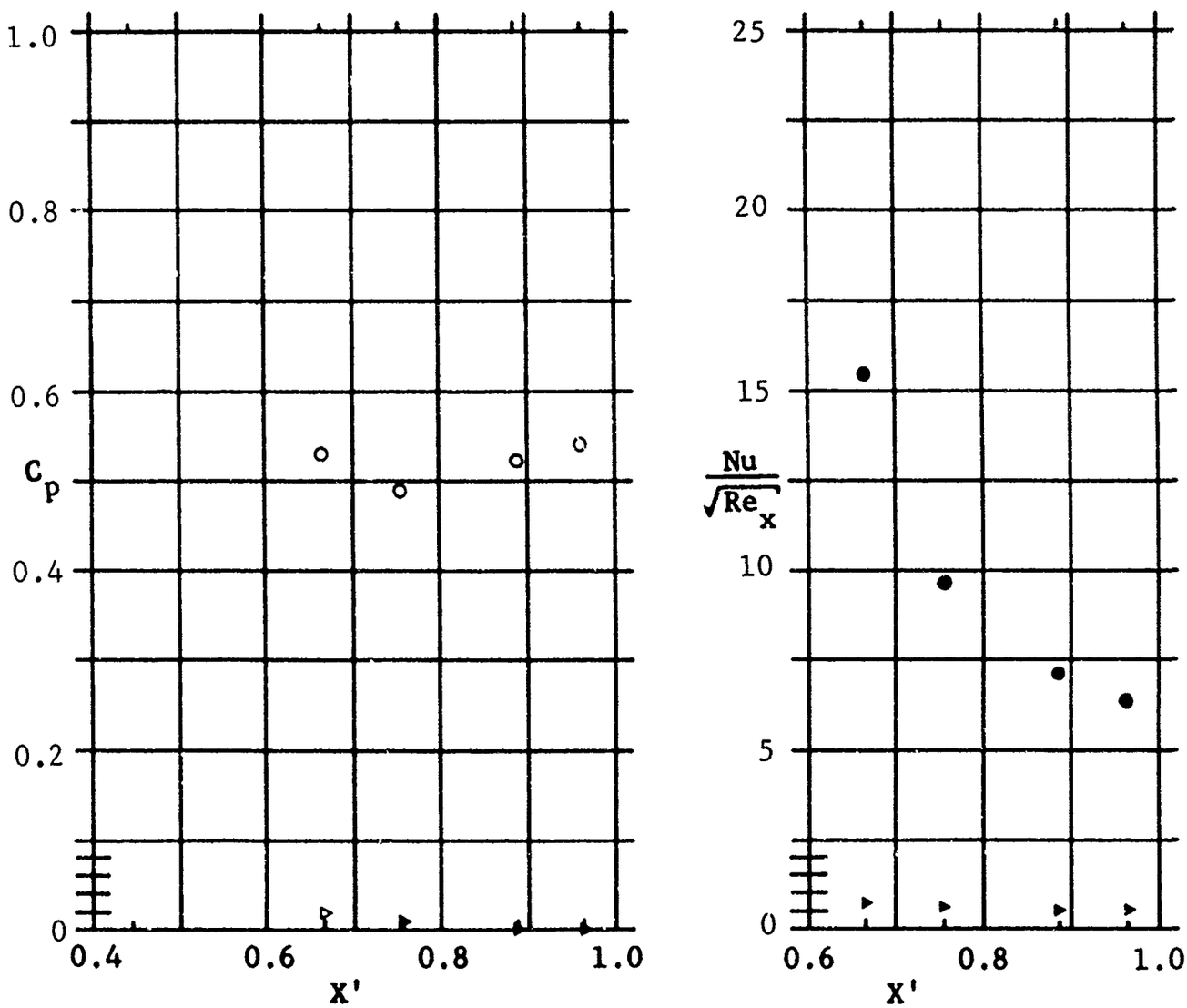

Fig. 23 C_p and $Nu/\sqrt{Re_x}$ versus X' for Basic Configuration with Ventral Fin at $\alpha = +30°$

Symbols	Gauge numbers and locations		
×	1 and 2	(lower surface),	Y' = 0
◆	3	(leading edge),	Y' = -0.449
▣	4	(leading edge),	Y' = 0.449
◎	5 thru 8	(lower surface),	Y' = 0.433
▶	9 thru 12	(upper surface),	Y' = 0.472
●	55 thru 58	(lower surface),	Y' = -0.433
▶	59 thru 62	(upper surface),	Y' = -0.472

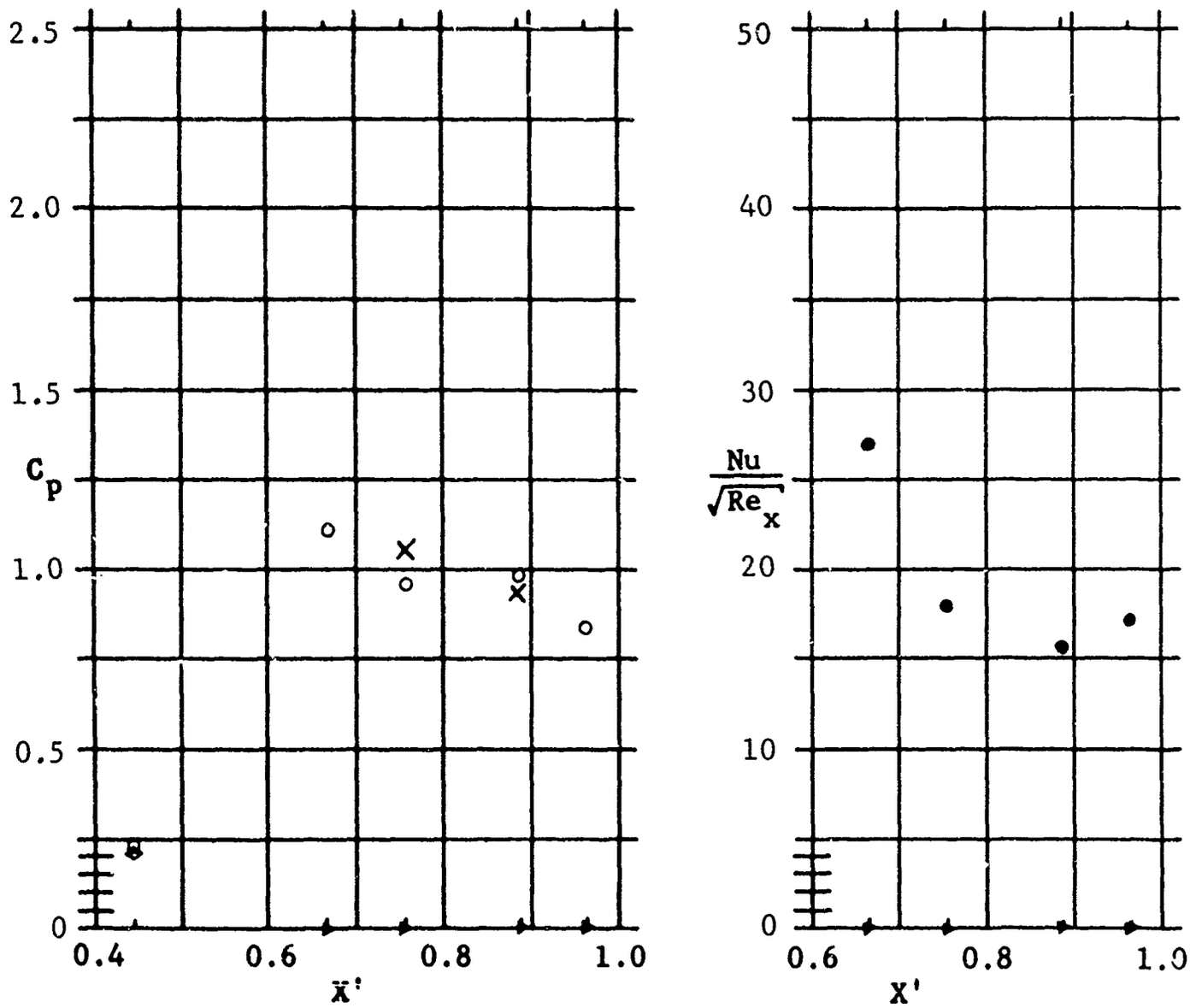

Fig. 24 C_p and $Nu/\sqrt{Re_x}$ versus X' for Basic Configuration at $\alpha = +45°$

Symbols	Gauge numbers and locations		
×	1 and 2	(lower surface),	Y' = 0
◈	3	(leading edge),	Y' = -0.449
⊡	4	(leading edge),	Y' = 0.449
⊙	5 thru 8	(lower surface),	Y' = 0.433
▶	9 thru 12	(upper surface),	Y' = 0.472
●	55 thru 58	(lower surface),	Y' = -0.433
▶	59 thru 62	(upper surface),	Y' = -0.472

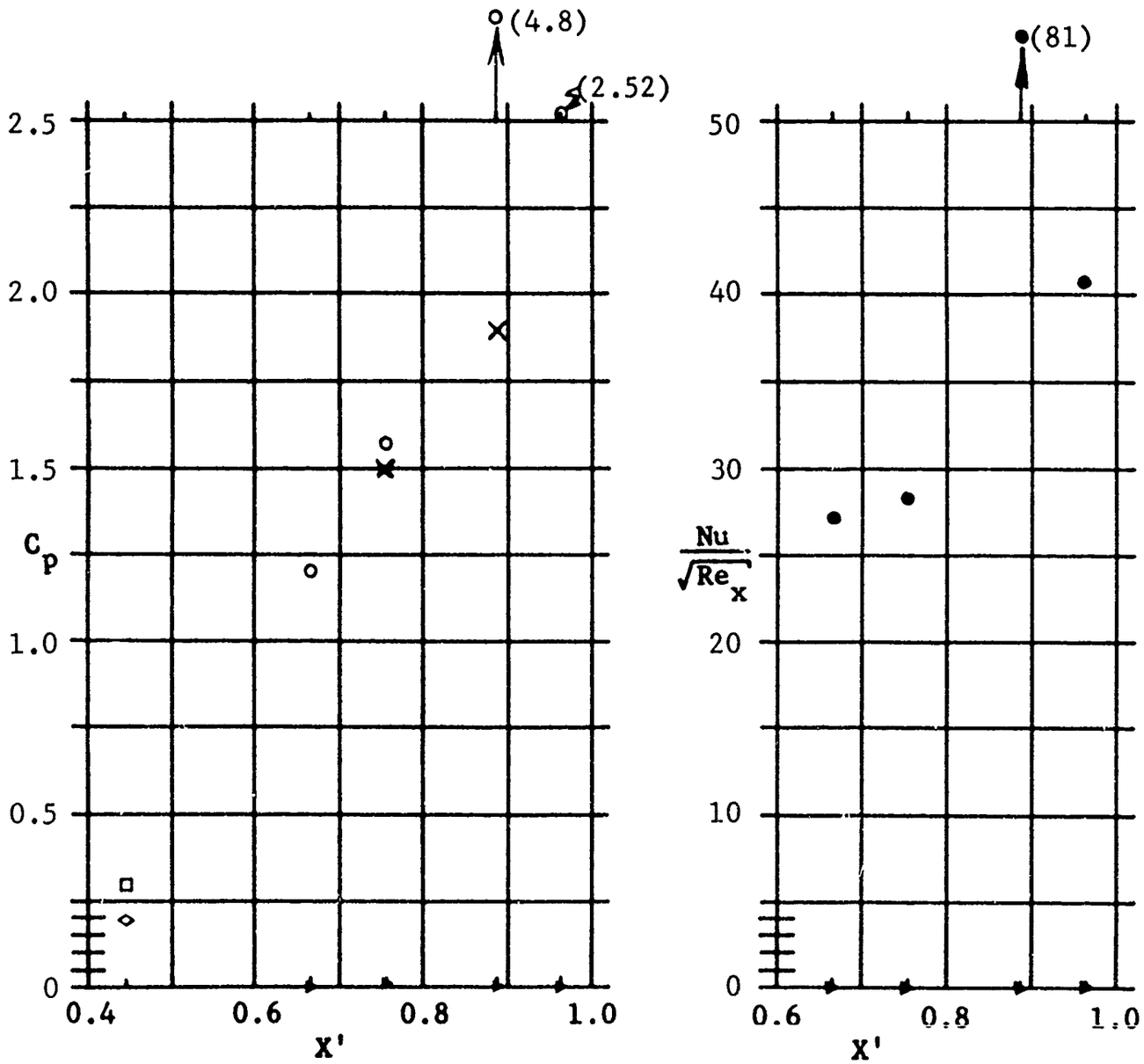

Fig. 25 C_p and $Nu/\sqrt{Re_x}$ versus X' for Basic Configuration with Lower Surface Flaps at $\alpha = +45°$

Symbols	Gauge numbers and locations		
×	1 and 2	(lower surface),	Y' = 0
◇	3	(leading edge),	Y' = -0.449
□	4	(leading edge),	Y' = 0.449
⊙	5 thru 8	(lower surface),	Y' = 0.433
▷	9 thru 12	(upper surface),	Y' = 0.472
●	55 thru 58	(lower surface),	Y' = -0.433
▶	59 thru 62	(upper surface),	Y' = -0.472

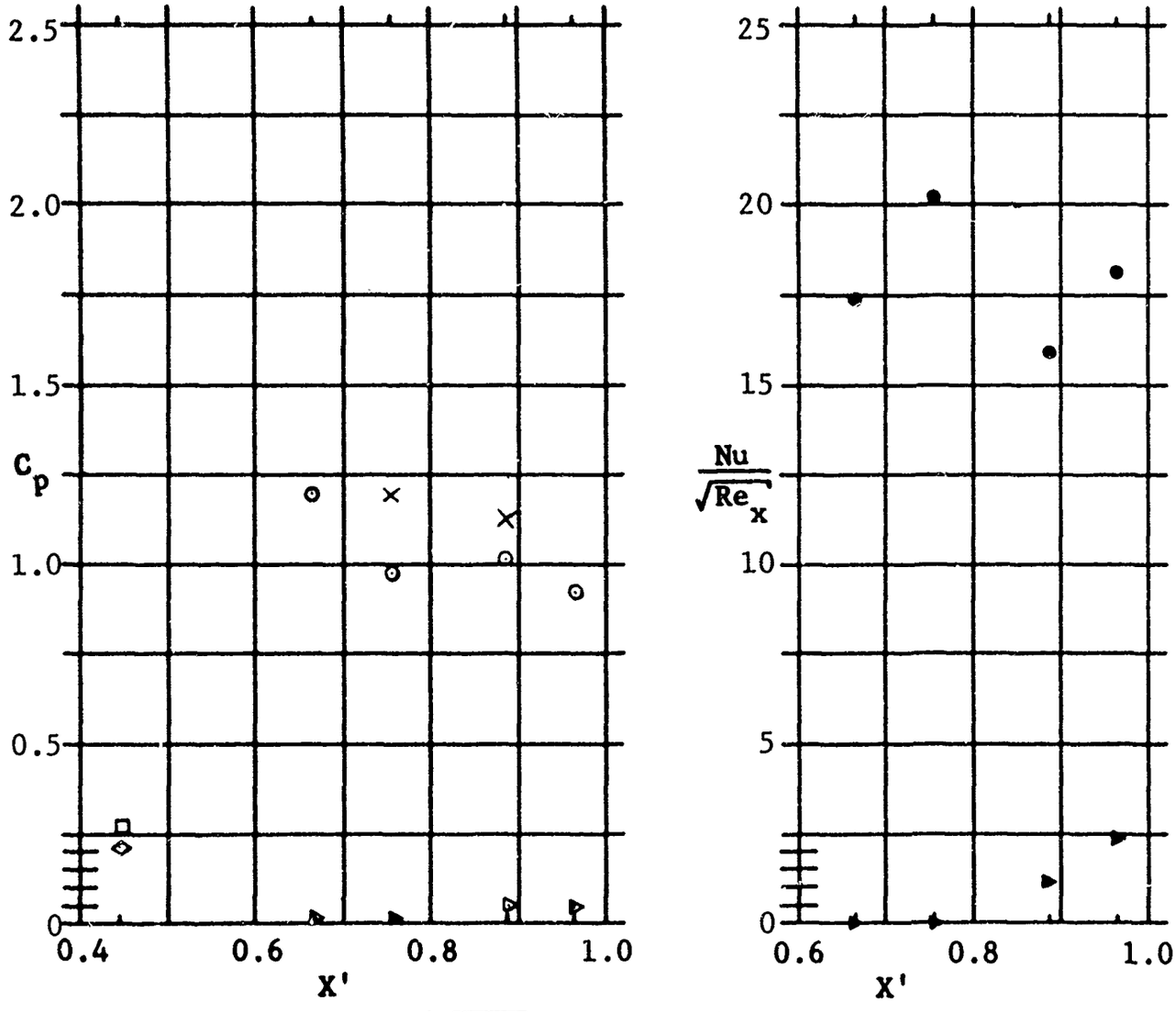

Fig. 26 C_p and $Nu/\sqrt{Re_x}$ versus X' for Basic Configuration with Upper (Dihedral) Surface Flaps at $\alpha = +45°$

Symbols	Gauge numbers and locations		
×	1 and 2	(lower surface),	Y' = 0
◈	3	(leading edge),	Y' = -0.449
⊡	4	(leading edge),	Y' = 0.449
⊙	5 thru 8	(lower surface),	Y' = 0.433
▶	9 thru 12	(upper surface),	Y' = 0.472
●	55 thru 58	(lower surface),	Y' = -0.433
▶	59 thru 62	(upper surface),	Y' = -0.472

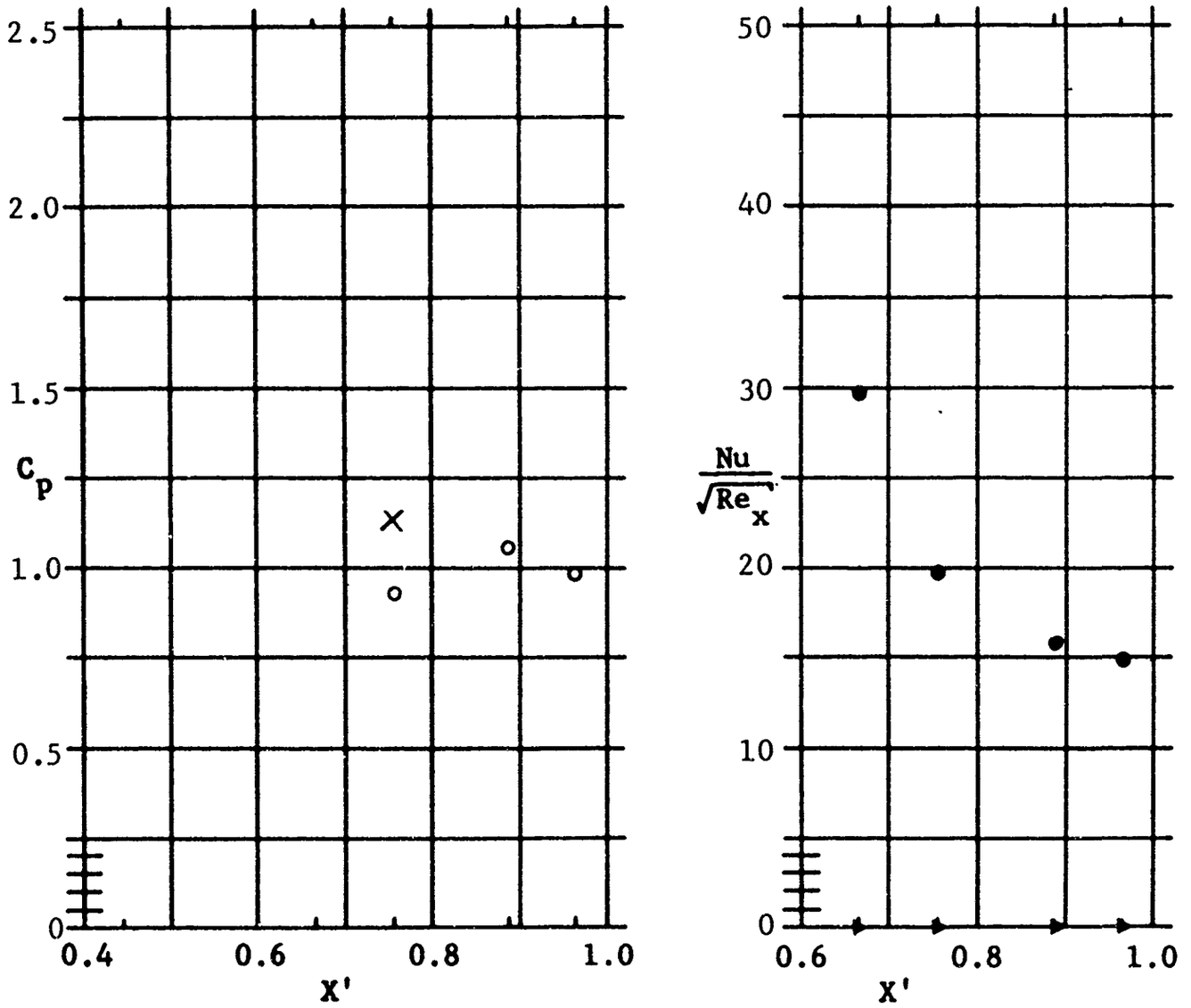

Fig. 27 C_p and $Nu/\sqrt{Re_x}$ versus X' for Basic Configuration with Ventral Fin at $\alpha = +45°$